Nascent RNA antagonises the interaction of a set of regulatory proteins with chromatin

Lenka Skalska[1,5,6], Victoria Begley[1,5], Manuel Beltran[1,5,7], Saulius Lukauskas[2], Garima Khandelwal[1], Peter Faull[3,8], Amandeep Bhamra[1], Manuel Tavares[1], Rachel Wellman[1], Andrey Tvardovskiy[2], Benjamin M. Foster[2,9], Igor Ruiz De Los Mozos[3,4], Javier Herrero[1], Silvia Surinova[1], Ambrosius P. Snijders[3], Till Bartke[2] and Richard G. Jenner[1,10]

[1]UCL Cancer Institute and Cancer Research UK UCL Centre, University College London (UCL), London, WC1E 6BT, UK.

[2]Institute of Functional Epigenetics, Helmholtz Zentrum München, Neuherberg, 85764, Germany.

[3]The Francis Crick Institute, London, NW1 1AT, UK.

[4]Institute of Neurology, UCL, London, WC1N 3BG, UK.

[5]These authors contributed equally.

[6]Present address: Barking, Havering and Redbridge University Hospitals NHS Trust, Romford, UK.

[7]Present address: Department of Biology and Biotechnology Charles Darwin, Sapienza University of Rome, Rome, Italy.

[8]Present address: College of Pharmacy, The University of Texas at Austin, Austin, Texas, 78712, USA.

[9]Present address: Department of Biochemistry, University of Oxford, Oxford, UK

[10]Lead Contact

Correspondence: r.jenner@ucl.ac.uk

SUMMARY

A number of regulatory factors are recruited to chromatin by specialised RNAs. Whether RNA has a more general role in regulating the interaction of proteins with chromatin has not been determined. We used proteomics methods to measure the global impact of nascent RNA on chromatin in embryonic stem cells. Surprisingly, we found that nascent RNA primarily antagonised the interaction of chromatin modifiers and transcriptional regulators with chromatin. Transcriptional inhibition and RNA degradation induced recruitment of a set of transcriptional regulators, chromatin modifiers, nucleosome remodelers, and regulators of higher-order structure. RNA directly bound to factors including BAF, NuRD, EHMT1 and INO80 and inhibited their interaction with nucleosomes. The transcriptional elongation factor P-TEFb directly bound pre-mRNA and its recruitment to chromatin upon Pol II inhibition was regulated by the 7SK ribonucleoprotein complex. We postulate that by antagonising the interaction of regulatory proteins with chromatin, nascent RNA links transcriptional output with chromatin composition.

INTRODUCTION

It is well established that transcription of DNA into coding and non-coding (nc)RNAs is regulated by proteins that respond to DNA sequence composition and chromatin state. It is also becoming clear that RNA molecules can themselves play a role in transcriptional and chromatin regulation. This was first demonstrated in mammalian cells for the transactivation response element (TAR), an RNA stem-loop formed at the 5′ end of nascent HIV transcripts, and for the cellular non-coding RNA, 7SK. TAR binds the HIV transactivator protein Tat and these factors act together to release positive transcription elongation factor b (P-TEFb) from the inhibitory 7SK ribonucleoprotein (RNP) complex to activate HIV transcriptional elongation (Barboric et al., 2007; Garber et al., 1998; Michels et al., 2003; Sedore et al., 2007; Wei et al., 1998; Yik et al., 2003). Since then, a number of long non-coding RNAs (lncRNAs) and enhancer RNAs (eRNAs) have been found to interact with transcriptional and chromatin regulatory proteins and modulate their recruitment or activity at specific sites on chromatin (Rinn and Chang, 2012).

In addition to the functions of specialised ncRNAs, RNA also acts in a global manner to regulate chromatin state. RNA and transcription impact higher-order structure across the genome (Barutcu et al., 2019; Heinz et al., 2018; Li et al., 2015; Saldana-Meyer et al., 2019). Building on models in which RNA forms a static nuclear matrix (Nickerson et al., 1989), it was more recently proposed that pre-mRNAs and other nascent transcripts form a dynamic nuclear RNA matrix that holds open active chromatin (Nozawa et al., 2017). Consistent with a more general role for RNA in chromatin regulation, recent studies demonstrate that chromatin regulators interact with a wide array of nascent transcripts. Although first identified to bind specific ncRNAs, Polycomb repressive complex 2 (PRC2), DNMT1 and DNMT3A, LSD1/KDM1A, CBX3, YY1, HDAC1 and CHD4 primarily interact with nascent pre-mRNAs

3

(Beltran et al., 2016; Hendrickson et al., 2016; Kaneko et al., 2013; Savell et al., 2016; Sigova et al., 2015). Similarly, unbiased screens for proteins interacting with nascent RNA or non-polyadenylated transcripts in cells have revealed enrichment for chromatin regulators (Bao et al., 2018; He et al., 2016; Trendel et al., 2019).

5

For the majority of factors identified to bind RNA in cells, the effect on their association with chromatin has not been determined. Although RNAs have primarily been considered to recruit regulatory proteins to chromatin, it has become apparent that nascent RNA can antagonise the association of proteins with chromatin. This is best understood for the repressive chromatin

10   modifier PRC2. PRC2 directly interacts with pre-mRNAs at essentially all active genes (Beltran et al., 2016; Davidovich et al., 2013; Kaneko et al., 2013) but preferentially binds G-quadruplex (G4)-forming sequences within these transcripts (Beltran et al., 2019; Kaneko et al., 2014; Wang et al., 2017a). In vitro, RNA competes with nucleosomes for PRC2 binding and inhibits PRC2 catalytic activity (Beltran et al., 2019; Beltran et al., 2016; Cifuentes-Rojas

15   et al., 2014; Herzog et al., 2014; Kaneko et al., 2014; Wang et al., 2017b; Zhang et al., 2019). In cells, blocking RNA polymerase II (Pol II) transcription (Hosogane et al., 2016; Kaneko et al., 2014; Riising et al., 2014) or degrading RNA (Beltran et al., 2016) triggers PRC2 recruitment to active genes. Reciprocally, blocking nuclear RNA degradation (Garland et al., 2019) or tethering G4-forming RNAs to repressed genes (Beltran et al., 2019) removes PRC2

20   from chromatin. Thus, pre-mRNA regulates its own production by preventing the recruitment of PRC2 to chromatin at active genes (Skalska et al., 2017). However, the broader impact of nascent RNA on the interaction of proteins with chromatin has not been determined.

We used proteomics methods to determine the effect of nascent RNA on the interaction of

25   proteins with chromatin in embryonic stem cells (ESC). Unexpectedly, we found that nascent

RNA primarily acted to inhibit the interaction of chromatin and transcriptional regulatory proteins with chromatin. We further demonstrate that nascent pre-mRNA directly binds to P-TEFb and that the 7SK RNP regulates the interaction of P-TEFb with nascent RNA and chromatin.

5

RESULTS

A set of regulatory proteins are recruited to chromatin upon transcriptional inhibition

We sought to determine the impact of Pol II transcription of nascent RNA on the association of proteins with chromatin using a stable isotope labeling with amino acids in cell culture (SILAC) based quantitative proteomics approach. Mouse ESC were treated with the TFIIH inhibitor triptolide, which blocks transcriptional initiation and leads to Pol II degradation, or the CDK9 inhibitor flavopiridol, which blocks transcriptional elongation, for 3 or 9 hrs (Figures 1A and S1A). These timepoints were chosen due to the previous observation that PRC2 was recruited to chromatin in ESC after 9 hrs of treatment with triptolide (Riising et al., 2014). RNA-seq revealed that flavopiridol and triptolide treatments had a greater effect on chromatin-associated nascent RNA (rRNA-depleted intronic reads) than on mature polyA+ exonic RNA and that transcription had largely ceased by 9 hours (Figures S1B and S1C). Chromatin fractions were purified and verified by silver-stain and immunoblotting (Figures S1D and S1E). The constituent proteins were then quantified by LC-MS/MS relative to chromatin from DMSO-treated cells at the same time point.

This analysis revealed a set of proteins lost from chromatin upon Pol II inhibition and, unexpectedly, a set of proteins recruited to chromatin upon Pol II inhibition (Figure 1B and Table S1). These changes were observed both upon treatment with flavopiridol and with triptolide ($r=0.66$, $p=2.9 \times 10^{-196}$, Pearson correlation and t-test) and similar changes were

evident at 3 and 9 hours, for both flavopiridol ($r=0.53$, $p=8\times10^{-108}$) and triptolide ($r=0.62$, $p=4.3\times10^{-162}$) (Figure S1F). The changes were not due to indirect effects of transcriptional inhibition on the cell cycle; treatment with flavopiridol and triptolide had similar effects on chromatin but opposite effects on the relative proportions of cells in G1 vs M phase (Figure S1G). Similarly, Pol II inhibition had little effect on apoptosis (Figure S1H) or DNA damage signalling (γH2A.X; Figure S1I), especially at the 3 hr timepoint. Similar effects could be observed after 1 hour treatment with flavopiridol and with a lower drug concentration (Figure S1J), again consistent with changes being a direct effect of transcriptional inhibition.

We first examined the set of proteins significantly depleted (FDR<0.05) from chromatin upon Pol II inhibition with both flavopiridol and with triptolide (9 hrs; n=241). As might be expected, this revealed enrichment of proteins with functions in RNA processing (GO:0006396; $p=8.9\times10^{-52}$, hypergeometric), including significant enrichment of subunits of the spliceosome, exosome, polyA complex, exon junction complex and Pol II-bound factors such as the PAF complex and SPT6/ISW1 (Figures 1B and S1K and Table S2). These proteins also included HNRNPU, previously shown to interact with chromatin in an RNA-dependent manner (Nozawa et al., 2017). Thus, these factors act as positive controls and suggest that the observed changes are caused by loss of Pol II transcription.

We then turned our attention to the set of proteins recruited to chromatin upon Pol II inhibition with both flavopiridol and triptolide (n=281). We found an enrichment of factors with roles in chromatin organisation (GO:0006325; $p=4\times10^{-5}$), gene expression (REAC:R-MMU-74160; $p=6\times10^{-4}$) and ESC pluripotency (WP:PluriNetWork; $p=5\times10^{-12}$) (Figures 1B and S1K and Table S2). A number of complexes exhibited a significant enrichment of subunits ($p<0.05$, hypergeometric), in the set of proteins recruited to chromatin upon Pol II inhibition (Figure 1C

and Table S2). These included PRC2, which has previously been shown to be recruited to chromatin upon transcriptional inhibition and RNA degradation (Beltran et al., 2016; Riising et al., 2014), other chromatin modifiers (DNMTs, EHMT1/2, MLL2/SET1A, HUSH), nucleosome remodelers (NuRD, NURF, NoRC, CHRAC, NuA4, INO80, BAF, ATRX/DAXX), regulators of higher-order structure (cohesin, CTCF, SMCHD1, SAFB), and transcription factors (including POU5F1 (OCT4), ZFP57, UBTF, TP53, MYBL2 and UTF1). Surprisingly, we also found that a number of regulators of Pol II processivity, including P-TEFb and other components of the super elongation complex (SEC), PPP2C1 (PP2A), BRD4, and Integrator, were recruited to chromatin upon Pol II inhibition, with P-TEFb exhibiting particularly large increases in chromatin association (Figure 1C). Immunoblotting for representative proteins in cell fractions generated using a different biochemical method confirmed Pol II inhibition induced changes in chromatin association for 16 of the 22 proteins tested (73%) and validated that changes in chromatin association were not an artefact of changes in total protein abundance (Figure 1D and Table S1).

We considered that if the changes in the association of proteins with chromatin were direct effects of changes in transcription, then restarting transcription should begin to reverse the changes. We therefore also analysed cells harvested 3 hrs after flavopiridol had been washed out after the initial 3 hr incubation (Figures 1E and S1L). This showed that removing flavopiridol and allowing transcriptional elongation to restart began to reverse the changes caused by flavopiridol treatment (r=-0.34, p=8.5×10^{-16}), although the magnitude of the effect was small relative to the initial treatment. Taking these data together, we conclude that transcription acts in a dynamic manner to regulate the association of a specific set of chromatin and transcriptional regulatory proteins with chromatin.

RNA degradation has similar effects to Pol II inhibition on the interaction of proteins with chromatin

Some of the changes observed upon transcriptional inhibition could reflect loss of nascent RNA but others could reflect loss of the process of transcription and its associated histone

5   modifications. That nascent RNA inhibits the association of PRC2 with chromatin is demonstrated by its recruitment to chromatin upon both Pol II inhibition (Riising et al., 2014) and RNaseA treatment (Beltran et al., 2016). Therefore, we considered that the effects of Pol II inhibition due to loss of nascent RNA should also be observed upon degradation of RNA in cells with RNaseA. To test this, we permeabilised ESC and either mock-treated or treated with

10   RNaseA. RNA-seq revealed that this reduced the level of chromatin-associated intronic transcripts by a median of 146-fold, but reduced polyA+ exonic RNA by only 1.3-fold (Figures S2A and S2B). The reason for this differential effect is unclear but may represent protection of mature mRNA by ribosomes or other RNA binding proteins.

15   We then quantified the change in protein association with the chromatin fraction using label-free LC-MS/MS (Figures 2A and S2C and Table S3). As we had observed upon inhibition of Pol II, RNA degradation caused loss of factors involved in RNA processing from chromatin and recruitment of a set of transcriptional and chromatin regulators (Figures 2B and Table S4). Taking the proteins altered by Pol II inhibition and comparing the changes with those caused

20   by RNA degradation revealed a significant correlation (r=0.45, p=4.9×10^{-28}, Figures 2C and S2D) and significant overlaps (Figure S2E; 47% proteins significantly depleted from chromatin after Pol II inhibition were also significantly depleted (FDR<0.05) from chromatin after RNaseA treatment (p=83×10^{-45}, hypergeometric); 24% of proteins significantly enriched on chromatin after Pol II inhibition were also significantly enriched (FDR<0.05) on chromatin

25   after RNaseA treatment (p=1.6×10^{-4})). Immunoblotting demonstrated that regulatory proteins

8

we had previously confirmed to be recruited to chromatin or depleted from chromatin in response to Pol II inhibition exhibited the same changes in chromatin association upon RNA depletion (Figure 2E).

5   Not all of the changes in chromatin composition induced by Pol II inhibition were recapitulated by RNA degradation. Indeed, for a minority of factors, RNA degradation had the opposite effect to Pol II inhibition. Rather than being recruited to chromatin, as occurred in response to Pol II inhibition, the THO complex and SAFB factors were lost from chromatin upon RNA degradation (Figure 2D), potentially indicating association with chromatin via stable RNAs.

10   Reciprocally, the PAF complex, which was depleted from chromatin upon Pol II inhibition, was recruited to chromatin upon RNA degradation (Figures S2F and S2G). We conclude that many of the changes in protein chromatin association caused by Pol II inhibition are recapitulated by RNA degradation, suggesting a role for nascent RNA, but that other changes are specific to one of the two treatment types.

15

RNA antagonises the interaction of a set of chromatin regulators with nucleosomes

Pol II inhibition and RNA degradation in cells are likely to have pleiotropic effects. Thus, we sought further evidence that RNA inhibited the interaction of chromatin regulatory proteins with chromatin. The antagonistic effect of transcription on the association of PRC2 with

20   chromatin reflects the inhibitory effect of RNA on PRC2 binding to nucleosomes (Beltran et al., 2019; Beltran et al., 2016; Wang et al., 2017b). We thus considered that RNA may also antagonise nucleosome binding by the other chromatin regulatory proteins identified in our proteomics analysis. To test this in an unbiased manner, we purified nuclear extract from ESC, either mock-treated the extract or treated it with RNaseA, incubated the extracts with

25   biotinylated dinucleosomes, purified the nucleosomes with streptavidin beads and then

quantified interacting proteins using SILAC (Figures 3A, S3A and S3B, and Table S5). We identified a set of proteins that exhibited increased binding and a set of proteins that exhibited decreased binding (FDR<0.05) to nucleosomes after RNA degradation (Figure 3B). Mirroring the effect of Pol II inhibition in cells, the GO term Chromatin Organisation was enriched (p=0.0017; Table S6) in the set of proteins that exhibited increased binding to nucleosomes after RNA degradation. Furthermore, there was a significant overlap between the sets of proteins that exhibited increased binding to nucleosomes after RNA degradation and those that exhibited increased association with chromatin upon Pol II inhibition (26% of proteins enriched on nucleosomes after RNA degradation *in vitro* were also enriched on chromatin after Pol II inhibition in cells (p=0.027; Figures 3C and S3C). However, differences were also noted. In addition to the chromatin regulators identified in the Pol II inhibition experiment, RNA depletion also increased nucleosome binding by the non-canonical PRC1 complex PRC1.6, the NSL and ATAC histone acetyltransferase complexes, and the NCOR1, NCOR2, CtBP/LSD1, MiDAC, SIN3A, ING2 and CAF-1 histone deacetylase complexes (Figure 3C), which were either under the significance threshold or were not detected in the cellular chromatin binding experiments.

To confirm the proteomics results, and to distinguish whether RNA inhibited the interaction of the proteins with the core nucleosome particle or with linker DNA, we repeated the experiment with either dinucleosomes, mononucleosomes incorporating linker DNA (185 bp), or mononucleosomes lacking linker DNA (147 bp) and measured changes in nucleosome interaction by immunoblotting (Figures 3D and S3D and Table S5). Of the 16 proteins we tested, 13 were enriched by nucleosome affinity purification and all of these exhibited increased nucleosome binding upon RNA degradation, including CHD1, CHD4, INO80, EHMT1, SMARCC1 and RUVBL2, thus validating the proteomics data. This experiment also

confirmed that RNA antagonised the interaction of PRC2 (SUZ12) with nucleosomes, which did not reach significance (FDR<0.01) in the proteomics analysis. In contrast, and also consistent with the proteomics data, HMGN1 exhibited decreased binding to nucleosomes upon RNA degradation. Furthermore, these results were apparent for all of the types of nucleosome tested, suggesting that RNA modulates the interaction of these factors with the core nucleosome particle rather than with linker DNA. We conclude that nuclear RNA inhibits the association of a set of regulatory proteins with nucleosomes, be this blocking direct interaction with nucleosomes or indirect interaction via a protein partner.

We next considered that if the increase in the binding of these proteins to nucleosomes after RNA degradation reflects antagonism of nucleosome binding by RNA, then this should be reversed by the re-addition of RNA. Because PRC2 promiscuously binds complex RNAs (Davidovich et al., 2013), tRNA can be used to model the competition between RNA and nucleosomes for PRC2 binding (Beltran et al., 2016). We therefore asked whether the increase in nucleosome binding of other chromatin regulators upon RNA degradation could also be reversed by the addition of tRNA. To test this, we added tRNA and RNase inhibitor to the RNaseA-treated nuclear extracts and repeated the nucleosome affinity purification and proteomics analysis (Figures 3E and S3E). We found that this generally reversed the changes in nucleosome binding caused by RNA degradation (r=-0.34, p=3.7x10^{-19}), demonstrating that RNA antagonises the interaction of this set of regulatory proteins with chromatin.

Direct interaction of chromatin regulators with RNA in cells

RNA inhibits the interaction of PRC2 with chromatin because it directly competes with nucleosomes for PRC2 binding (Beltran et al., 2019; Beltran et al., 2016; Wang et al., 2017b). Thus, we asked whether the antagonistic effect of RNA on the interaction of regulatory complexes with chromatin could reflect direct interaction between these proteins and RNA. To

11

test this, we selected a set of eight proteins representative of the factors that exhibited increased chromatin binding after RNA degradation; the NuRD component CHD4, the INO80 component INO80, the INO80 and NuA4 component RUVBL2, the BAF components SMARCC1 and SMARCA4, EHMT1, the HMG box transcription factor UBTF, and the integrator subunit INTS11 and used CLIP to determine whether these proteins directly bound RNA in cells. We detected direct RNA binding for six of these eight proteins in cells (Figure 4A and S4). This was evidenced by detection of an RNP of the expected molecular weight, with a smear of trimmed RNA extending above, which was stronger in the +UV and +PNK conditions and which diminished as the RNaseI concentration was increased.

To explore this on a more global scale, we compared the sets of proteins that were depleted or recruited to chromatin upon Pol II inhibition with proteins identified to bind RNA in twelve previous screens, eight of which identified proteins bound to mature polyadenylated RNA (Baltz et al., 2012; Beckmann et al., 2015; Castello et al., 2012; Castello et al., 2016; Conrad et al., 2016; Kwon et al., 2013; Mullari et al., 2017; Perez-Perri et al., 2018) and four of which could also identify proteins bound to nascent RNA or other non-polyadenylated transcripts (Bao et al., 2018; Caudron-Herger et al., 2019; He et al., 2016; Trendel et al., 2019). We found that the set of proteins depleted from chromatin was significantly enriched for RBPs identified by all of the studies (Figure 4B). Then, focusing on the set of proteins recruited to chromatin upon Pol II inhibition, we found this was significantly enriched for RBPs identified by all four studies that could measure non-polyadenylated RNA binding, including a study that specifically identified proteins bound to nascent RNA (Bao et al., 2018). The set of proteins recruited to chromatin upon Pol II inhibition was also enriched for RBPs identified by three of the eight studies that were limited to polyA+ RNA, albeit to a lesser extent. Taken together

with our CLIP data, these results suggest that the inhibitory effect of RNA on the interaction of these proteins with chromatin is due to the interaction of these factors with RNA.

P-TEFb interacts with nascent pre-mRNA in cells

The P-TEFb subunits CDK9, CyclinT1 and CyclinT2 were amongst the proteins exhibiting the greatest increases in chromatin association upon Pol II inhibition and RNaseA treatment (Figures 1C and 2D). We hypothesised that the antagonistic effect of RNA on P-TEFb chromatin binding could reflect interaction of P-TEFb with RNA. Consistent with this possibility, CyclinT1 directly contacts HIV TAR RNA when in a complex with HIV Tat (Garber et al., 1998; Richter et al., 2002; Wei et al., 1998). We first tested whether P-TEFb bound to RNA in ESC by performing iCLIP for P-TEFb using an antibody specific to CDK9. This resulted in co-precipitation of CyclinT1 and revealed a UV-dependent RNP that matched the molecular weight of CyclinT1 (Figure S5A). This RNP could also be observed by CLIP with an antibody to CyclinT1 (Figure S5B) and was depleted upon degradation of CDK9 using THAL-SNS-032, demonstrating it to be dependent on P-TEFb (Figure S5C). We conclude that P-TEFb interacts with RNA in cells. Although the size of the RNP corresponds to CyclinT1, we can't rule out that other proteins that interact with P-TEFb also contribute to this signal.

Sequencing of P-TEFb RNA crosslink sites revealed strong enrichment for 7SK RNA (Figure S5D), as expected given its role in sequestering P-TEFb. However, we found that the majority of P-TEFb crosslinks mapped to protein-coding genes with enrichment around 5' splice sites (5'SS) that was not observed in the background RNA crosslinking from input control samples (Figures 5A and S5E). CLIP for CDK9 did not co-precipitate the 7SK RNP component LARP7 (Figure S5F) and crosslinking around 5'SS was not observed in iCLIP experiments for LARP7 (Figures 5A and S5G) demonstrating that P-TEFb was not binding to pre-mRNA as part of the

7SK RNP. iCLIP for P-TEFb did not enrich for snRNAs, suggesting that the crosslinking detected around 5'SS does not reflect co-precipitation of spliceosome components (Figure S5D).

5   Given the enrichment of P-TEFb RNA crosslinking around 5'SS, we considered that P-TEFb binding to RNA might be dependent on splicing. To test this, we compared P-TEFb crosslinking at 5'SS at exons included in the mature transcript versus exons that were excluded (Figures 5B and S5H). We found that P-TEFb RNA crosslinking was only apparent at included exons, consistent with this crosslinking being dependent on splicing. Furthermore, P-TEFb

10   exhibited reduced crosslinking to RNA transcribed from single-exon compared to multi-exon genes (Figure S5I). To confirm a requirement for splicing, we repeated CDK9 iCLIP after treatment of cells with the SF3b inhibitor pladienolide B (pla-B, 1 μM for 6 hours) (Figure 5C). We found that the specific pattern of P-TEFb crosslinking around 5'SS was not observed after treatment with pla-B and conclude that P-TEFb directly binds nascent pre-mRNA around

15   5'SS and that this is dependent on splicing.

7SK RNA regulates the interaction of P-TEFb with nascent RNA and chromatin

We sought to understand the factors that regulate the interaction of P-TEFb with RNA or chromatin. P-TEFb is held in a poised state by the 7SK RNP, from which it is released to

20   activate transcriptional elongation (Bacon and D'Orso, 2019; Quaresma et al., 2016). The lack of enrichment of the core 7SK RNP component LARP7 with nascent RNA indicated that P-TEFb interacted with nascent RNA in its free, non-7SK associated, form. We considered that if this was the case then depletion of 7SK RNA should increase P-TEFb binding to nascent RNA. To test this, we performed CLIP for P-TEFb in ESC transfected with antisense LNA

25   oligonucleotides specific for 7SK RNA or scrambled control oligos (Figures 6A and S6A). We

found that knockdown of 7SK increased P-TEFb RNA binding (p=0.008, Welch's t-test) but, in contrast, had no effect on binding of LARP7 to RNA. This demonstrates that P-TEFb binds nascent RNA in its free form, and this is countered by its interaction with 7SK.

5 Given that 7SK antagonised the association of P-TEFb with nascent RNA, we hypothesised that the transfer of P-TEFb to chromatin upon Pol II inhibition might also be regulated by 7SK (transcribed by Pol III). To test this, we measured the effect of Pol II inhibition on P-TEFb association with chromatin in WT HAP1 cells and in HAP1 cells in which *7SK* is deleted (Studniarek et al., 2021). We found that treatment with triptolide increased P-TEFb association

10 with the chromatin fraction in WT cells but not in 7SK knockout (KO) cells (p<0.05, Student's t-test, Figures 6B and 6C). In contrast, SMARCC1 increased in the chromatin fraction in both WT and 7SK KO cells, while LARP7 showed no change. Thus, 7SK is required for recruitment of P-TEFb to chromatin upon Pol II inhibition.

15 The 7SK RNP associates with chromatin at active genes through interaction with KAP1 (McNamara et al., 2016). We therefore considered that the transfer of P-TEFb to chromatin upon Pol II inhibition might depend on KAP1. To test this, we measured the effect of triptolide treatment on P-TEFb chromatin association in WT and KAP1 KO cells. We found that in the absence of KAP1, the extent of P-TEFb recruitment to chromatin was approximately halved

20 (p<0.05, Student's t-test, Figures 6D and 6E), indicating that the association of 7SK with genes facilitates P-TEFb recruitment to chromatin upon Pol II inhibition. We explored whether the requirement for 7SK and KAP1 for P-TEFb recruitment to chromatin upon Pol II inhibition was because P-TEFb became associated with 7SK on chromatin. However, CyclinT1 immunoprecipitation from the chromatin fraction revealed a reduction in P-TEFb interaction

25 with 7SK RNA and LARP7 after Pol II inhibition (Figure S6B). Thus, 7SK is necessary for

transfer of P-TEFb to chromatin upon transcriptional inhibition but does not itself constitute the chromatin-associated P-TEFb pool in transcriptionally inactive cells. Taken together, these data support a model in which nascent RNA binds to a set of transcriptional and chromatin regulators and inhibits their association with chromatin, which, in the case of P-TEFb, is regulated by the 7SK RNP (Figure 6F).

DISCUSSION

The antagonistic effect of RNA on the interaction of PRC2 with chromatin has been demonstrated by experiments employing Pol II inhibition, RNA degradation and nucleosome-RNA competition assays (Beltran et al., 2019; Beltran et al., 2016; Riising et al., 2014; Wang et al., 2017b). By adapting these methods to allow a more systematic analysis, we have revealed that the antagonistic effect of nascent RNA on PRC2 function is an example of a broader role for RNA in inhibiting the interaction of transcriptional and chromatin regulator proteins with chromatin. That nascent RNA inhibits the association of DNMT1 and DNMT3A with chromatin is consistent with previous data demonstrating that RNA inhibits the activity of these enzymes (Di Ruscio et al., 2013; Hendrickson et al., 2016; Savell et al., 2016), while the identification of BAF is consistent with previous reports that RNA inhibits its interaction with nucleosomes (Cajigas et al., 2015; Han et al., 2014; Jegu et al., 2019; Prensner et al., 2013). That RNA inhibits the interaction of Cohesin with chromatin is potentially consistent with previous findings that transcription inhibition induces Cohesin accumulation at intragenic sites (Heinz et al., 2018). RNA has not previously been reported to antagonise the interaction of other proteins identified here with chromatin, although a number of the factors have previously been found to bind RNA, including MLL/SET complexes (Wang et al., 2011), BRD4 (Rahnamoun et al., 2018), Integrator (Baillat et al., 2005), INO80 subunits (Davidovic et al., 2006; Jeon and Lee, 2011; Sigova et al., 2015), NuRD (Hendrickson et al., 2016; Zhao et al.,

16

2016), NoRC and CHRAC (Hu et al., 2019; Mayer et al., 2006), Cohesin (Hendrickson et al., 2016; Li et al., 2013; Pan et al., 2020; Tsai et al., 2018), CTCF (Hansen et al., 2019; Kung et al., 2015; Saldana-Meyer et al., 2014), SMCHD1 (Chen et al., 2015) and SAFB (Rivers et al., 2015). The set of proteins identified to be antagonised by RNA is enriched for functions in

5   ESC pluripotency and a number of the factors share subunits and/or function together in common pathways, for example PRC2 with NuRD (Reynolds et al., 2012) and INO80 (Xue et al., 2017), suggesting that nascent RNA regulates the interaction of factors with chromatin in a coordinated manner.

10   Of the factors we identified to be regulated by nascent RNA, we focused on P-TEFb because its subunits were amongst the proteins exhibiting the greatest increases in chromatin association upon Pol II inhibition and because it had previously been shown to directly bind HIV TAR RNA (Garber et al., 1998; Richter et al., 2002). The Pol II Ser-2 kinases Ctk1 and Bur1 have also been found to directly bind nascent RNA in *S. cerevisiae*, suggesting that

15   nascent RNA binding activity is conserved in eukaryotes (Battaglia et al., 2017). However, in yeast, RNaseA treatment reduced, rather than increased, the association of Ctk1 and Bur1 with chromatin (Battaglia et al., 2017), potentially reflecting differences in the mechanisms of chromatin association between species.

20   Our discovery that nascent pre-mRNA interacts with P-TEFb and antagonises its association with chromatin suggests that cellular pre-mRNA may act in an analogous manner to TAR, which releases the Tat:P-TEFb complex from the 7SK RNP (D'Orso and Frankel, 2010). The RNA binding proteins SRSF2 (Ji et al., 2013), DDX21 (Calo et al., 2015), WDR43 (Bi et al., 2019) and RBM7 (Bugai et al., 2019) have all been found to release P-TEFb from 7SK and

25   increase Pol II Ser-2P and thus may act in an analogous manner to Tat. In particular, SRSF2

both promotes splicing and P-TEFb recruitment to genes (Ji et al., 2013; Lin et al., 2008), which is potentially consistent with the requirement for splicing for P-TEFb binding to 5'SS.

Further studies will be required to ascertain the importance of nascent RNA binding for P-TEFb function. Interaction of P-TEFb with nascent pre-mRNA could increase the size of the free P-TEFb pool or could specifically direct its activities to particular locations or substrates. For example, P-TEFb binding to internal sites within pre-mRNA could function to maintain Ser-2P as Pol II travels through the gene body. More specifically, the splicing-dependent enrichment of P-TEFb at 5'SS may help couple splicing with transcriptional elongation (Herzel et al., 2017) and may contribute to previously observed stimulatory effects of splicing on Ser-2P and transcriptional elongation (Caizzi et al., 2021; Chathoth et al., 2014; Fong and Zhou, 2001; Ji et al., 2013; Koga et al., 2015; Lin et al., 2008).

Limitations of the Study

We recognise that Pol II inhibition and RNA degradation likely have pleiotropic effects on the cell and thus we sought to identify changes in protein chromatin association that were common to both treatments and also complemented these cellular treatments with measurement of the effect of RNA depletion from nuclear extracts on the interaction of proteins with nucleosomes. Pol II inhibition and RNA degradation had a greater effect on nascent transcripts than on mature polyA+ RNA species, suggesting that changes in the interaction of proteins with chromatin are primarily due to loss of nascent RNA, but it is possible that some of the effects are caused by loss of short-lived mature RNAs. The experimental design also does not distinguish between the effects of pre-mRNAs versus other nascent RNA species. However, it is likely that much of the effect is due to pre-mRNAs because these represent the majority of nascent and chromatin-associated RNAs in the cell (Mondal et al., 2010; Nozawa and Gilbert, 2019; St

Laurent et al., 2012) and, where known, the majority of RNAs bound by the factors identified here, including PRC2 (Beltran et al., 2016), DNMT1 (Hendrickson et al., 2016), DNMT3A (Savell et al., 2016), the NuRD components CHD4 and HDAC1 (Hendrickson et al., 2016) and P-TEFb (this study). Further work will be necessary to determine the RNA species bound by the factors identified, the binding sites on chromatin impacted by RNA, and the importance of RNA binding activity for the function of the proteins in the cell. In the case of P-TEFb, further work is necessary to identify the factor(s) that mediate its association with chromatin upon Pol II inhibition.

In summary, our work demonstrates that nascent RNA regulates the interaction of a set of chromatin and transcriptional regulatory factors with chromatin and primarily acts to antagonise their interaction with chromatin. These results are consistent with models in which nascent RNA provides direct feedback from gene transcription to chromatin state (Skalska et al., 2017) and provides evidence of a close interplay between RNA and chromatin in gene regulation. Nascent RNAs and other transcripts have been proposed to contribute to a dynamic matrix or phase-separated compartments that regulate chromatin state (Hnisz et al., 2017; Nozawa and Gilbert, 2019). Thus, these structures may function in part by concentrating the antagonistic effects of RNA at regions of active chromatin in the cell.

ACKNOWLEDGEMENTS

AUTHOR CONTRIBUTIONS

DECLARATION OF INTERESTS

The authors declare no competing interests.

FIGURE LEGENDS

Figure 1. A set of regulatory proteins are recruited to chromatin upon transcriptional inhibition

a. Experimental strategy. ESC were treated with DMSO, flavopiridol or triptolide for 3 or 9 hrs, the chromatin fractions purified, and proteins quantified relative to DMSO by SILAC.

b. Significance (q-value/FDR) of changes in the association of proteins with chromatin upon treatment with flavopiridol (left) or triptolide (right) versus DMSO at 9 hrs. The GO term RNA processing (blue) was significantly enriched ($p=8.9 \times 10^{-52}$, hypergeometric) in the set of proteins depleted from chromatin (FDR<0.05) in both treatments. The GO term Chromatin organisation (red) was significantly enriched ($p=4 \times 10^{-5}$) in the set of proteins recruited to

20

chromatin (FDR<0.05). Proteins with these functions are highlighted and their frequencies within the sets of proteins recruited or depleted from chromatin shown above.

c. Proteins that exhibited significantly increased abundance in the chromatin fraction upon Pol II inhibition with flavopiridol and triptolide (9 hrs). Protein complexes are labelled if a significant proportion of their subunits were increased on chromatin (p<0.05, hypergeometric). Interactions between proteins (STRING) are shown as lines. Changes in chromatin association of individual proteins upon treatment with flavopiridol are indicated by color, according to the scale on the right, and by the outline (black FDR<0.05, white FDR>0.05).

d. Immunoblots for proteins representative of those shown in c. in the cytoplasmic, nucleoplasmic and chromatin fractions and whole cell extract (WCE) taken from ESC after 0, 3 or 6 hrs incubation with flavopiridol.

e. Top, Strategy: After the 3 hr-incubation, flavopiridol was washed out, cells incubated for a further 3 hrs and then harvested. Bottom: Proteins either recruited to or depleted from chromatin (FDR<0.05) upon treatment with flavopiridol at the 3 hr timepoint (n=519) ordered by the change in chromatin binding (average of 3 and 9 hr timepoints). Changes in chromatin association induced by flavopiridol washout (relative to 3 hr flavopiridol) are shown below and are anti-correlated with the changes initially induced by flavopiridol (r=-0.34, 8.5×10^{-16}, n=519). Changes in chromatin association are colored according to the scale beneath.

See also Figure S1 and Tables S1 and S2.

Figure 2. RNA degradation has similar effects to Pol II inhibition on the interaction of proteins with chromatin

a. Experimental strategy. ESC were permeabilised, mock-treated or treated with RNaseA to degrade RNA, chromatin fractions purified, and proteins quantified by label-free LC-MS/MS.

b. Significance of changes in the association of proteins with chromatin upon RNaseA treatment versus mock-treated control. Proteins with functions in RNA processing and chromatin organisation are highlighted in blue or red, respectively, and their frequencies in the sets of proteins recruited or depleted from chromatin (FDR<0.05) shown above.

c. Changes in the association of proteins with chromatin upon Pol II inhibition (average of 9 hr flavopiridol and triptolide data) and RNA degradation relative to their respective control samples (scale below). Proteins were either recruited to chromatin or depleted from chromatin after both flavopiridol and triptolide treatments. The change in protein chromatin association in response to RNA degradation is shown below and is correlated ($r=0.45$, $p=4.9 \times 10^{-28}$, $n=527$).

d. Change in chromatin association caused by RNA degradation for the proteins and complexes shown in Figure 1C. Details as for 1C.

e. Immunoblots for proteins representative of those shown in d. in the cytoplasmic, nucleoplasmic and chromatin fractions and WCE purified from ESC after mock treatment (-) or treatment with RNaseA (+).

See also Figure S2 and Tables S3 and S4.

Figure 3. RNA antagonises the interaction of a set of chromatin regulators with nucleosomes.

a. Experimental strategy. ESC nuclear extract was mock-treated or treated with RNaseA and incubated with biotinylated dinucleosomes, which were then purified by streptavidin affinity purification and bound proteins quantified by SILAC.

b. Significance of changes in the association of proteins with nucleosomes upon RNaseA treatment versus mock-treated control. Proteins with functions in RNA processing and chromatin organisation are highlighted in blue or red, respectively, and their frequencies in the

22

sets of proteins that showed decreased or increased nucleosome binding (FDR<0.05) shown above.

c. Chromatin modifiers and nucleosome remodeler complexes that exhibit a significant number of subunits with increased nucleosome binding after degradation of RNA in nuclear extract. Changes in the association of proteins with nucleosomes vs the mock treated sample are indicated by color, according to the scale on the right, and by the outline (black FDR<0.05, white FDR>0.05). Proteins detected in the Pol II inhibition experiment but not this experiment are in grey.

d. Immunoblots for proteins representative of those shown in c. in nucleosome pull-downs (dinucleosomes, or mononucleosomes assembled with 187 or 147 bp DNA) from mock-treated (-) or RNaseA-treated (+) nuclear extracts.

e. Top: strategy: tRNA and RNase inhibitor were added to nuclear extracts after RNAseA-treatment. Bottom: Proteins exhibiting either significantly increased or decreased interaction with nucleosomes after RNaseA degradation. Change in nucleosome interaction after tRNA addition is shown below and is anti-correlated (r=-0.34, p=3.7×10^{-19}, n=668).

See also Figure S3 and Tables S5 and S6.

Figure 4. Direct interaction of chromatin regulators with RNA in cells.

a. SDS-PAGE for RNPs enriched by CLIP for CHD4, INO80, RUVBL2, SMARCC1, EHMT1, UBTF and non-specific IgG controls in ESCs. Autoradiograms of crosslinked ^{32}P-labelled RNA are shown at the top; the corresponding immunoblots below. CLIP was performed with and without UV crosslinking and polynucleotide kinase (PNK) and with high (H; 40 U/ml) or low (L; 4 U/ml) concentrations of RNase I. The arrows indicate the molecular weight of the protein of interest.

b. Proportion of proteins exhibiting a significant increase on chromatin (FDR<0.05, n=281), decrease on chromatin (FDR<0.05, n=241) or no change on chromatin (FDR>0.05, n=617) upon treatment with flavopiridol and triptolide (9 hrs) that were identified to bind RNA in the indicated studies. Studies are divided into those that could only detect binding to polyA+ RNA and those that could also detect binding to non-polyA+ RNA. For each study, significance is estimated relative to the proportion of non-changing proteins identified to bind RNA (binomial test with Bonferroni correction).

See also Figure S4.

Figure 5. P-TEFb directly interacts with nascent pre-mRNA in cells.

a. Average P-TEFb (red), LARP7 (blue) and background input (black) RNA crosslinking around 5' splice sites (SS) at first and mid exons and 3' SS at mid and last exons within nascent RNAs at all genes.

b. Average P-TEFb (red) band background input (black) RNA crosslinking around 5' SS at excluded and included exons.

c. Average P-TEFb RNA crosslinking at 5' SS in cells treated with DMSO or pladienolide B (Pla-B).

See also Figure S5.

Figure 6. 7SK RNA regulates the interaction of P-TEFb with nascent RNA and chromatin.

a. Left: SDS-PAGE for RNPs enriched by CLIP for P-TEFb and LARP7 in ESC transfected with scrambled ASO or ASO specific for 7SK RNA. Autoradiograms of crosslinked RNA are shown at the top; immunoblots below. Right: Quantification of the change in RNA crosslinking (7SK ASO vs scrambled ASO) relative to protein (mean and S.D, n=7 (P-TEFb) or n=2 (LARP7), 1-sided Welch's t-test).

b. Immunoblots for CyclinT1 (CCNT1), CDK9, LARP7, SMARCC1 and control proteins in cytoplasmic, nucleoplasmic and chromatin fractions and WCE from WT and 7SK KO HAP1 cells after incubation with triptolide for 0, 3 and 6 hours.

c. Quantification of immunoblots shown in b. measuring chromatin association of each protein relative to t=0 (mean and S.D., 1-sided Student's t-test, 3 independent experiments).

d. Immunoblots in cytoplasmic, nucleoplasmic, and chromatin fractions and WCE from WT and KAP1 KO HEK293T cells after incubation with triptolide for 0, 3 and 6 hours.

e. Quantification of immunoblots shown in e. measuring chromatin association of each protein relative to t=0 (mean and S.D., 1-sided Student's t-test, 3 independent experiments).

f. Model: Nascent RNA binds a set of transcriptional and chromatin regulators and antagonises their association with chromatin. For some of these factors, RNA inhibits their interaction with nucleosomes. For P-TEFb, RNA binding and recruitment to chromatin are regulated by the 7SK RNP.

See also Figure S6.

STAR METHODS

RESOURCE AVAILABILITY

5   **Lead contact**

Further information and requests for resources and reagents should be directed to and will be fulfilled by the lead contact, Richard G. Jenner (r.jenner@ucl.ac.uk).

Materials availability

10   This study did not generate new unique reagents.

Data and code availability

The SILAC mass spectrometry proteomics data have been deposited to the ProteomeXchange Consortium via the PRIDE (Perez-Riverol et al., 2019) partner repository with the dataset

15   identifier PXD018706. The label-free mass spectrometry proteomics data have been deposited to the ProteomeXchange Consortium via the PRIDE (Perez-Riverol et al., 2019) partner repository with the dataset identifier PXD018641. iCLIP and RNA-seq data have been deposited in the Gene Expression Omnibus (GEO) with accession code GSE150677. Raw immunoblotting and autoradiogram images have been deposited in Mendeley Data at

20   http://dx.doi.org/10.17632/67dcgtbks5.1.

EXPERIMENTAL MODEL AND SUBJECT DETAILS

25   All cells were cultured at 37°C in 5% CO_2. Cell lines were not authenticated. Mouse E14 ESC (male) (Hooper et al., 1987) were maintained on 0.1% gelatin in KO-DMEM, 10% FCS, 5% knockout serum replacement, non-essential amino acids, L-glutamine, 2-mercaptoethanol,

penicillin-streptomycin and 1000 U/ml leukemia inhibitory factor (Amsbio #AMS-263-100).

For Pol II inhibition and nucleosome IP mass spectrometry studies, media was supplemented

with 100 mg/l lysine K8 CNLM-291-H, 100 mg/l arginine R10 CNLM-539-H or 100 mg/l light

amino acids (K0 and R0) (ThermoFisher #89989 #89987), and 100 mg/l proline. Cells were

5   maintained for 6 passages (~14 doublings) to ensure full amino acid incorporation and were

assayed for alkaline phosphatase activity (ThermoFisher #A14353). WT and 7SK KO HAP1

cells (haploid male) (kind gift from Sylvain Egloff; Studniarek et al., 2021) were maintained

in Iscove's Modified Dulbecco's Medium (IMDM) with 10% FCS and penicillin/streptomycin.

WT and KAP KO HEK293T cells (female; kind gift from Helen Rowe; Tie et al., 2018) were

10   maintained in DMEM, 10% FCS and penicillin-streptomycin. ESC, HAP1 and HEK293T cells

were incubated at 37°C and treated with triptolide (10 µM, Sigma T3652), flavopiridol (10

µM, Sigma F3055), or an equivalent volume of DMSO, for the times indicated. For reversal of

transcriptional inhibition induced by flavopiridol, after 3 hr of treatment, ESC were washed

twice with warm medium and incubated for a further 3 hrs. ESC were treated with 1 µM

15   pladienolide B (Santa Cruz sc-391691) or an equal volume of DMSO for 6 hrs.

METHOD DETAILS

Experiments were not performed blinded. Samples were not randomised.

20

Cell fractionation for proteomics experiments

For the Pol II inhibition experiments, heavy and light labeled ESC were treated with triptolide

and flavopiridol as described above. For the RNA degradation experiments, RNaseA treatment

25   was performed as described (Beltran et al., 2016). ESC were trypsinized, washed twice with

PBS, permeabilized with 0.05% Tween-20 in PBS for 10 min on ice, washed once, resuspended

with PBS and mock-treated with 1 U/µl SUPERase.In (Invitrogen AM2694) or treated with 1

µg/µl RNaseA (Sigma R6513) for 30 min at RT. Chromatin fractions were then purified as

described (Monte et al., 2012). Cells were then centrifuged at 1200 rpm, washed twice with PBS, and re-suspended in a hypotonic lysis buffer, (10 mM Tris pH 7.5, 15 mM NaCl, 0.15% v/v NP-40) with protease and phosphatase inhibitors (10 mM sodium butyrate, 0.1 mM PMSF, 0.2 mM Na_3VO_4, 0.1 mM NaF, Complete protease inhibitor and 1 U/ μl Superase.In) and incubated on ice for 5 min. Cells were then centrifuged at 4,000 rpm for 5 min at 4 °C and the cytoplasmic supernatant harvested. The nuclear pellet was re-suspended in hypotonic lysis buffer and layered gently onto a sucrose cushion (24% sucrose (w/v), 10 mM Tris pH 7.5, 15 mM NaCl with protease/phosphatase inhibitors and 1 U/μl Superase.In), centrifuged for 10 min at 5,000 rpm and washed with PBS. Isolated nuclei were then resuspended in 20 mM HEPES (pH 7.6), 7.5 mM $MgCl_2$, 30 mM NaCl, 1 M urea, 1% NP-40 with protease/phosphatase inhibitor and 1 U/μl Superase.In and incubated for 10 min on ice to extract soluble proteins. Samples were then centrifuged at 13,000 rpm for 10 min to pellet the insoluble chromatin and the soluble nucleoplasmic fraction removed. The chromatin pellet was washed with PBS and proteins extracted in 50 mM Tris (pH 8), 1 mM EDTA, 0.05% SDS with protease/phosphatase inhibitors and treated with 250 units of benzonase (Sigma E1014) in the presence of 2 mM $MgCl_2$ for 1 hr. Buffer was then added to give a final concentration of 50 mM Tris (pH 8), 10 mM EDTA, 1% SDS with protease/phosphatase inhibitors and incubated at RT for 10 min. Insoluble material was removed by centrifugation at 13,000g for 15 mins at 4°C and the supernatant harvested.

Nucleosome affinity purification for proteomics

Heavy and light labeled ESC were trypsinised, collected by centrifugation and washed with PBS. Cell pellets were resuspended in 10 volumes of hypertonic buffer (10 mM Hepes pH 7.9, 1.5 mM $MgCl_2$, 10 mM KCl, 0.5 mM DTT and Complete protease inhibitor) for 10 mins on ice. Cells were recovered by centrifugation at 1500g for 5 mins and the pellet resuspended in

3 volumes of hypertonic buffer supplemented with 0.1% IGEPAL CA-360 and incubated for 10 mins at 4°C. Nuclei were pelleted by centrifugation at 1500g for 5 mins and resuspended in 5 mM Hepes pH 7.9, 26% glycerol, 250 mM NaCl, 1.5 mM MgCl$_2$, 0.2 mM EDTA, 0.5 mM DTT and Complete protease inhibitor. The NaCl concentration was then slowly increased to 400 mM and nuclear extraction carried out for 1 hr at 4 °C with occasional agitation. Insoluble material was removed by centrifugation (13.000rpm, 20 min at 4 °C) and soluble nuclear extracts cleared using a Proteus clarification column (Generon #MSF500). Protein concentration was measured using Pierce BCA (ThermoFisher Scientific 23225). Nuclear extracts were then treated with 1 μg/μl RNaseA (Sigma R6513) or mock treated with PBS with 1 U/μl RNaseOUT (Invitrogen 1077019) for 30 mins at 1100 rpm at 37°C. The RNaseA treated sample was then split and half treated with 1 U/μl RNaseOUT and half with 1 U/μl RNaseOUT and 2 μg/μl tRNA (Invitrogen AM7119). Histone octamers were assembled into dinucleosomes by salt deposition dialysis using a biotinylated 382 bp DNA fragment containing the 601 nucleosome-positioning sequence, as described (Makowski et al., 2018). 2.5 μg of dinucleosomes were incubated with 12.5 μl of previously washed Streptavidin Dynabead T1 (Invitrogen 65601) in SNAP Buffer (20 mM HEPES pH 7.9, 150 mM NaCl, 0.2 mM EDTA (pH 8.0), 1 mM DTT, 20% Glycerol, 0.1%, IGEPAL CA-630, plus Complete protease inhibitor) for 1 hr at 4°C. Complexes were washed twice in SNAP buffer and then incubated with 1.2 mg of mock-treated or RNAseA-treated nuclear extract in SNAP buffer with a final volume of 1 ml. The binding reaction was allowed to proceed for 3 hrs at 4°C, beads were then washed twice in SNAP buffer and twice in SNAP buffer without IGEPAL CA-630. Nucleosomes were resuspended in 50 μl elution buffer (100 mM Tris pH 7.5, 2 M Urea, 10 mM DTT) and incubated for 20 mins at 25°C at 1100 rpm.

SILAC

For the Pol II inhibition experiments, protein extracts were quantified by BCA. 25 μg of heavy and light labeled samples were mixed to give a total of 50 μg protein. 25 μg of heavy or light-labeled flavopiridol or triptolide-treated samples were mixed with DMSO-treated samples from the same timepoint labeled with the alternative amino acids. Heavy labeled samples were also mixed with the equivalent light labeled samples as controls. Heavy or light-labeled flavopiridol washout samples were mixed with alternatively-labeled 3 hr flavopiridol, 3 hr DMSO or washout samples. Mixes were loaded onto separate lanes of a 10% NuPAGE gel (Invitrogen) and run approx. 10 mm. Each lane was manually excised, diced into ~1 mm³ pieces and transferred to a single well of a flat-bottomed 96-well plate. A Janus liquid handling robot (Perkin Elmer) was used to de-stain, reduce (10 mM dithiothreitol) and alkylate (55 mM iodoacetamide) proteins prior to overnight trypsin digest (100 ng, Pierce Trypsin Protease, MS Grade) at 37 °C. The following day, peptides were extracted using 50% acetonitrile, 1% formic acid. Peptide samples were dried by vacuum centrifugation then re-solubilised in 0.1% trifluoroacetic acid prior to mass spectrometry analysis.

For the nucleosome affinity purification experiments, equal volumes of affinity-purified proteins from the heavy or light-labeled RNaseA-treated samples were mixed with the proteins purified from the alternatively-labeled mock-treated samples or with alternatively-labeled RNaseA treated samples as controls. Iodoacetamide (Sigma I1149) was added to a final concentration of 50 mM and samples incubated for a further 10 mins at 25ºC at 1100 rpm in the dark. Proteins were digested by addition of 0.3 μg trypsin (Promega V5113) at 25ºC for 2 hrs at 1100 rpm. Samples were pelleted, the supernatant collected and a second trypsinization performed using 50 μl of elution buffer for 5 mins at 25ºC. The supernatant was again collected, combined with the previous sample, and digested by incubation with 0.3 μg of trypsin

overnight at 25ºC and 1100 rpm. The reaction was then stopped with 0.5% TFA (Sigma), samples desalted using C18 Stage tips and eluted in 60 % acetonitrile.

A Thermo Fisher Scientific UltiMate 3000 UHPLC instrument loaded peptide samples onto a trap cartridge (Acclaim PepMap 100 C18, 300 μm inner diameter, 5 mm length, 5 μm particle size) for desalting. Peptides were transferred to an EASY-Spray analytical column (PepMap C18, 50 μm inner diameter, 15 cm length, 2 μm particle size, 100 Å pore size) and separated using a 120-minute gradient of increasing organic solvent (80 % acetonitrile, 5 % dimethyl sulfoxide) from 8 to 40 %. An orbitrap Fusion Lumos Tribrid (Thermo Fisher Scientific) mass spectrometer was operated in positive ionisation mode to acquire data. Instrument settings were: MS1 data were acquired in the orbitrap at a resolution of 120k, 4E6 AGC target, 50 milliseconds maximum injection time, dynamic exclusion of 60 seconds, a mass range of 300-1500 m/z and profile mode data capture. MS2 data were acquired in the ion trap using a 2 m/z isolation window, 2E4 AGC target, 300 milliseconds maximum injection time (inject ions for all available parallelisable time "Universal Method"), 35 % collision-induced dissociation (CID) energy, 10 milliseconds activation time and centroid mode data capture.

Label-free quantification (LFQ)

Chromatin fractions from RNaseA-treated and mock-treated cells were collected from 4 independent experiments, loaded onto separate wells of a NuPAGE gel (Invitrogen) and run until fully resolved. The gel was cut horizontally into five sections to facilitate quantification by molecular weight across lanes. Bands from each lane were excised and diced into 1 mm^3 pieces. Gel pieces were washed with 50% acetonitrile and water. Proteins were reduced with 10 mM dithiothreitol in 100 mM ammonium bicarbonate at 56°C for 45 min and alkylated with 55 mM iodoacetamide in 100 mM ammonium bicarbonate at ambient temperature for 30 mins

in the dark. Gel pieces were washed again as before. Proteins were digested with 300 ng trypsin at 37°C overnight. Peptides were extracted with 50% and 100% acetonitrile washes. Samples were evaporated to dryness at 30°C and resolubilised in 0.1% formic acid. LC-MS/MS was performed on a Q Exactive Orbitrap Plus interfaced to a NANOSPRAY FLEX ion source and coupled to an Easy-nLC 1200 (Thermo Scientific). Thirty five percent of each sample was analysed as 7 µl injections. Peptides were separated on a 24 cm fused silica emitter, 75 µm diameter, packed in-house with Reprosil-Pur 200 C18-AQ, 2.4 µm resin (Dr. Maisch) using a linear gradient from 5% to 30% acetonitrile/0.1% formic acid over 120 min at a flow rate of 250 nl/min. Peptides were ionised by electrospray ionisation using 1.8 kV applied immediately prior to the analytical column via a microtee built into the nanospray source with the ion transfer tube heated to 320°C and the S-lens set to 60%. Precursor ions were measured in a data-dependent mode in the orbitrap analyser at a resolution of 70,000 and a target value of 3e6 ions. The ten most intense ions from each MS1 scan were isolated, fragmented in the HCD cell, and measured in the orbitrap at a resolution of 17,500.

Cell fractionation for validation experiments

To validate changes in chromatin association upon Pol II inhibition and RNA degradation detected by LC-MS/MS, ESC were treated with triptolide, flavopiridol or RNaseA as described above. Cell fractionation was performed as described previously (Beltran et al., 2016; Zoabi et al., 2014). Cells were centrifuged at 1200 rpm, washed twice with PBS and 20% of the cells separated for use as WCE. The remaining cells were re-suspended in 1 ml of buffer A (10 mM HEPES (pH 7.9), 10 mM KCl, 1.5 mM MgCl2, 0.34 M sucrose, 10% glycerol, 1 mM DTT with Complete protease inhibitor). Triton X-100 (0.1%) was added, and the cells were incubated for 5 min on ice. Nuclei were collected by low-speed centrifugation (4 min, 1,300g, 4°C). The supernatant (cytoplasmic fraction) was further clarified by high-speed centrifugation

(15 min, 20,000g, 4 °C). Nuclei were washed twice in buffer A, and then lysed in buffer B (3 mM EDTA, 0.2 mM EGTA, 1 mM DTT, Complete protease inhibitor). Insoluble chromatin was collected by centrifugation (4 min, 1,700g, 4°C), and the supernatant (nucleoplasm) harvested. The final chromatin pellet (insoluble chromatin fraction) was washed twice with buffer B and proteins extracted in 50 mM Tris (pH 8), 1 mM EDTA, 0.05% SDS with Complete protease inhibitor and 250 units of benzonase in the presence of 2 mM $MgCl_2$ for 1 hr. Buffer was then added to give a final concentration of 50 mM Tris (pH 8), 10 mM EDTA, 1% SDS with Complete protease inhibitor and incubated at RT for 10 min. Insoluble material was removed by centrifugation at 13,000g for 15 mins at 4°C and the supernatant harvested. The experiments were performed in duplicate.

Nucleosome affinity purification validation

Recombinant human histones were expressed in *E. coli* and purified as described (Makowski et al., 2018). Histone octamers were assembled into mononucleosomes and dinucleosomes by salt deposition dialysis using biotinylated 147, 185 and 382 bp DNA fragments containing the 601 nucleosome-positioning sequence. 1.25 µg dinucleosomes pre-bound to Streptavidin Dynabead T1 or equimolar amount of mononucleosomes were incubated with 50 µg of mock or RNAseA-treated nuclear extract in SNAP buffer with a final volume of 250 µl. The binding reaction was allowed to proceed for 3 hrs at 4°C, beads were then washed 3 times in SNAP buffer and nucleosomes resuspended in NuPAGE protein loading buffer. The experiment was performed in duplicate.

Immunoblotting

Cell fractions and extracts were quantified by BCA (Pierce). Samples were boiled in Laemmli buffer or NuPAGE buffer and equal amounts (10 µg) of cell fractions (equal volumes for

33

immunoprecipitates) were loaded for each treatment. When blotting for Pol II phospho-forms, cells were lysed in TOPEX+ buffer (50 mM Tris-HCl pH7.5. 300 mM NaCl, 0.5% Triton X-100, 1% SDS, 1 mM DTT, 1x Complete protease inhibitor (Roche), 5 mM NaF, 0.2 mM Na_3VO_4,10 mM β-glycerophosphate, and 33 U/ml benzonase (EMD-Novagen). Proteins were resolved by SDS-PAGE with size markers (ThermoFisher) and transferred to nitrocellulose membranes (GE Healthcare). Proteins were detected with primary antibodies to DNMT3A (Abcam ab2850), TRRAP (Abcam ab73546), SET (Abcam ab181990), LMNA (Abcam ab26300), HMGN1 (Bethyl Laboratories A302-263), UTF1 (Abcam ab24273), CDK9 (Abcam ab6544), beta-Tubulin (Abcam ab6064), RUVBL2 (Abcam ab36569), SF3A3 (Bethyl Laboratories A302-506A), ZFP57 (Abcam ab45341), FUS (Novus Biologicals 100-565), LARP7 (Novus biologicals A303-723A), ILF3 (Abcam ab92355), CyclinT1 (Abcam ab184703), UBTF (Santa Cruz sc-13125), KAP1/TRIM28 (Abcam ab3831), SUZ12 (Santa Cruz sc-46264), LEO1 (Bethyl Laboratories A300-174A), HNRNPU (Abcam ab10297), EHMT1 (Abcam ab41969), STAG1 (Abcam ab4457), STAG2 (Abcam 4463), SMARCC1 (Abcam ab172638), BRD4 (Santa Cruz sc-48772), INO80 (ProteinTech 18810-1-AP), CHD1 (Cell Signalling D8C2), CHD4 (Abcam ab70369), CHD8 (Bethyl A301-224A), P300 (Santa Cruz sc-585), KDM2A/JHDM1A (Bethyl A301-475A), MPP8 (Santa Cruz sc-398598), Pol II S2P (Abcam ab5095), Pol II S5P (Millipore 05-623), total Pol II (Santa Cruz sc-899), Beta-actin (Cell Signalling 4967S), histone H3 (Abcam ab1791) and γH2A.X (Ser139) (clone JBW301) (Sigma 05-636-I). Proteins were visualised using Amersham ECL western blotting detection reagent (GE) and detected using an ImageQuantLAS 4000 imager and ImageQuantTL (GE). Contrast and brightness were altered in a linear fashion equally across the whole image. Proteins exhibit changes in chromatin association or nucleosome binding that were not validated by immunoblotting are indicated in Tables S1, S3 and S5.

7SK knockdown

ESC were trypsinized and nucleofected with 1 nmole of scrambled or 7SK ASO (Flynn et al., 2016) per $2x10^6$ ESC using the Amaxa 4D-Nucleofector X Unit (Lonza VPH-1001) with the Amaxa 4D-Nucleofector Protocol for Mouse ESC. After nucleofection, cells were re-plated and cultured for 8 hrs. RNA was purified using TRIsure (Bioline BIO-38033) according to the manufacturer's instructions and reverse transcribed with SuperScript III (ThermoFisher) using random hexamer primers. Enrichment of cDNAs compared to input control was measured by qPCR (Applied Biosystems) using QuantiTect SYBR Green PCR kit (Qiagen 204143) with primers for 7SK 5'-AGAACGTAGGGTAGTCAAGC -3' and 5'-AGAAAGGCAGACTGCCACAT -3' and Actb 5'-TCTTTGCAGCTCCTTCGTTG-3' and 5'-ACGATGGAGGGGAATACAGC-3'. The experiment was repeated 7 times.

CLIP

CLIP was performed as described (Huppertz et al., 2014) with the following differences: cells were irradiated with 0.2 J/cm^2 of 254 nm UV light in a Stratalinker 2400 (Stratagene). $5x10^6$ cells were used per IP and were lysed in 1 ml of lysis buffer with Complete protease inhibitor (Roche). Lysates were passed through a 27 G needle, 4 U/ml of DNase Turbo (Ambion AM2238) and RNase I (Ambion AM2294, range between 1-20 U/ml) added, and incubated in a thermomixer at 37 °C and 1100 rpm for 3 minutes. 5 µl of α-RUVBLl2 (Abcam ab36569), 5 µg α-UBTF (Santa Cruz sc-13125), 5 µg α-INO80 (ProteinTech 18810-1-AP), α-CHD4 (Abcam ab70369), α-SMARCC1 (Abcam ab172638), α-EHMT1 (Abcam ab41969), α-CDK9 (Santa Cruz sc-484), α-LARP7 (Bethyl A303-723A), α-SMARCA5/SNF2H (Abcam ab3749), α-INTS11 (Bethyl A301-274A), α-CCNT1 (Abcam ab238940), α-CDK9 (Santa Cruz sc-484), α-LARP7 Bethyl A303-723A) or non-specific IgG (Abcam ab46540) antibody was used per experiment and bound to 50 µl of pre-washed Dynabeads protein G beads (Invitrogen

10003D) for 1 hr at RT. Antibody-bound beads were then incubated with lysate for 5 hrs at 4 °C. Beads were washed 3 times with 900 µl of high-salt buffer (supplemented with 1 M urea) and twice with 900 µl of wash buffer. After transfer, the membrane was washed twice with 1x PBS, exposed overnight to a phosphoimager screen (Fuji), and visualised with an Amersham Typhoon Trio image scanner. Protein and RNA bands were quantified with ImageJ. CLIP experiments were performed in duplicate.

iCLIP

iCLIP was performed as described (Huppertz et al., 2014) with variations from (Beltran et al., 2016). Cells were irradiated with 0.2 J/cm^2 of 254 nm UV light in a Stratalinker 2400 (Stratagene), 6-10x10^7 cells were used per IP. Cells were lysed in 1 ml of lysis buffer, lysates passed through a 27 G needle and sonicated for 3x 10s pulses with a Diagenode Picoruptor. 200 U/ml of DNase Turbo (Ambion), and 4 U/ml of RNase I (Ambion) were added and lysates incubated in a thermomixer at 37°C and 1100 rpm for 3 mins. Lysates were cleared by centrifugation and Proteus clarification spin columns, according to the manufacturer's instructions. 5 µg of antibody was used for each CLIP (CDK9 Santa Cruz sc-484; LARP7 Bethyl A303-723A). After SDS-PAGE and transfer to membrane, cross-linked RNPs between 80 and 110 kDa (CyclinT1) or 70 to 100 kDa (LARP7) were isolated. iCLIP for the CyclinT1 input sample was performed as described (Beltran et al., 2016), extracting RNPs between 80-110 kDa. RNA was purified and after reverse transcription, cDNA was fractionated by running samples on a precast 6% TBE-urea gel at 180 V for 40 mins and cDNA bands running between 120-180 nt (high), 85-120 nt (medium) and 70-85 nt (low) isolated. One µl of each fraction was pooled to optimize the number of cycles in the PCR, determined by the minimum number of cycles that produced detectable amplicon in gels stained with SYBR Green I (Invitrogen S7585). Once the optimal number of optimal cycles was established, the library PCR was

performed separately for each fraction, checked by gel electrophoresis and pooled in equal proportions. Library concentration was determined using the KAPA Universal Library Quantification kit (Roche KK4824), according to the manufacturer's instructions and library concentration was corrected by multiplication by 0.38 to account for insert size. Single-end 50-bp reads were generated on a HiSeq 2500.

Co-immunoprecipitation from chromatin

ESC were treated with 10 μM triptolide or an equivalent volume of DMSO for 6 hours, trypsinized and the chromatin fraction purified as described (Beltran et al., 2016; Zoabi et al., 2014). Chromatin was resuspended in 50 mM Tris (pH 8), 1 mM EDTA and 20 U/ml of DNase Turbo (Ambion AM2238) for 30 min at RT, followed by the addition of 0.5% sodium deoxycholate and sonication for 10 x 30s pulses with a Diagenode Picoruptor. Once the chromatin fraction was completely dissolved, IP buffer (20 mM Tris-HCl, 0.5% NP-40, 150 mM NaCl, 1.5 mM MgCl2, 10 mM KCl, 10% Glycerol, 0.5 mM EDTA, pH 7.9, 1 mM DTT, Complete protease inhibitor and 1 U/μl RNaseOUT (Invitrogen 1077019)) was added up to 1 ml and centrifuged for 5 min at 13,000 rpm to pellet any insoluble material. 50 μl of the sample was saved as input and the remaining sample pre-cleared with Protein G Dynabeads at 4ºC for 1 hr. The beads were removed, each sample divided into two, and incubated with 2.5 μg of anti-CCNT1 (Abcam ab238940) or non-specific IgG for 16 hours. Samples were then incubated with Protein G Dynabeads at 4ºC for 2 hours. Beads were washed 5 times with IP buffer and centrifuged for 5 min at 1,000 rpm at 4ºC to remove any remaining supernatant. Laemmli buffer was added to half the beads and inputs and processed for immunoblotting and the other halves were resuspended in TRIsure for RNA purification. RNA was treated with DNase Turbo and reverse-transcribed with the ImProm-II Reverse Transcription System (Promega A3800) using random hexamer primers. Enrichment of 7SK versus 5S rRNA was

measured by qPCR (Applied Biosystems) using QuantiTect SYBR Green PCR kit (Qiagen) with primers for 7SK 5'-AGAACGTAGGGTAGTCAAGC-3' and 5'-AGAAAGGCAGACTGCCACAT-3' and 5S rRNA 5'-AAGCCTACAGCACCCGGTAT-3' and 5'-GATCTCGGAAGCTAAGCAGG-3'. The experiment was repeated 3 times.

RNA-seq

ESC were mock or RNaseA treated or treated with 10 μM triptolide or flavopiridol for 0, 1, 3 or 9 hours. For whole cell extract RNA, cells were resuspended in TRIsure. For chromatin-associated RNA, cells were fractionated as described (Werner and Ruthenburg, 2015) with minor modifications. Cells were re-suspended in 1 ml of buffer A (10 mM HEPES (pH 7.9), 10 mM KCl, 1.5 mM MgCl2, 0.34 M sucrose, 10% glycerol, 1 mM DTT with Complete protease inhibitor), triton X-100 (0.1%) added, and the cells were incubated for 5 mins on ice. Nuclei were collected by low-speed centrifugation (4 min, 1,300g, 4°C) and washed twice in buffer A. The pellet was resuspended in 250 μl NUN buffer (20 mM HEPES pH 7.6, 300 mM NaCl, 1M Urea, 1% NP-40, 7.5 mM MgCl2, 1 mM DTT, with protease inhibitor) and incubated for 10 mins on ice, then centrifuged (1,400g, 4 min, 4°C). The resulting pellet was washed twice with buffer A and an equal volume of TRI Reagent (Sigma T3934) was added to the chromatin pellet. Before RNA extraction, we spiked-in 5% of drosophila cells resuspended in TRIsure into the whole cell extract RNA samples and 1% into the chromatin-associated RNA samples. RNA was purified following the manufacturer´s protocol and treated with DNase Turbo. Libraries were generated from WCE RNA by polyA selection and from chromatin-associated RNA library by rRNA depletion and sequenced by GENEWIZ.

Cell cycle, caspase activation, cell death, γH2A.X

ESC were treated with triptolide or flavopiridol as above, or with 10 nM SN-38 (Sigma H0165) for 24 hrs. Cells were then trypsinized and resuspended in media. Cell viability was measured

using eF780 (Invitrogen 65-0865-14) in triplicate. Caspase-3 and -7 activation was measured in duplicate using the Vybrant FAM Caspase-3 and -7 assay kit (Invitrogen V35118) following the manufacturer's instructions with a BD LSR Fortessa X-20. For cell cycle analysis, cells were fixed with 70% ethanol, washed with PBS and incubated with 100 μg/ml RNaseA (Sigma)

5   and 25 μg/ml propidium iodide from the sVybrant FAM Caspase kit for 10 mins at RT. Cells were then analysed by flow cytometry in triplicate and the data averaged. For γH2A.X analysis, cells were treated with triptolide or flavopiridol as above, or with 10 μM doxorubicin (Sigma D1515), and whole cell extract purified. The experiment was performed 3 times.

10   **QUANTIFICATION AND STATISTICAL ANALYSIS**

Statistical tests used and n are stated upon first use in the results text and in the figure legends.

Mass-spectrometry data analysis

SILAC: Raw data were analysed in MaxQuant v1.6.0.13 (Cox and Mann, 2008) and searched

15   against a UniProt *Mus musculus* protein database downloaded 14/06/2012 using default settings. A SILAC quantification method (multiplicity 2) using light amino acid labels (K0 and R0) and heavy labels (K8 and R10) was selected. Carbamidomethylation of cysteines was set as fixed modification, and oxidation of methionines and acetylation at protein N-termini were set as variable modifications. Enzyme specificity was set to trypsin with maximally 2 missed

20   cleavages allowed. MaxQuant generated a reverse database for decoy searching and an internal protein contaminant database was also searched containing sequences including trypsin and keratins. A 1% FDR at the protein and peptide level was selected.

LFQ: Raw data were analysed in MaxQuant v1.5.2.8 and searched against the same UniProt

25   database. Label-free quantification was selected with a match time window of 0.7 min, an

alignment time window of 20 min to quantify the proteins with the 'match between runs' feature selected. Other settings were the same as for SILAC.

LC-MS/MS data post-processing and analysis

5 The 'proteinGroups.txt' quantification files were used for statistical data analysis and the Pol II inhibition, RNase-treated chromatin and RNase-treated nucleosome affinity purification experiments processed separately. Proteins marked as *Potential contaminant, Only identified by site, Reverse* by MaxQuant and proteins with less than two peptides identified were excluded. The remaining proteins were classified into nuclear and non-nuclear proteins based

10 on subcellular location information in UniProt (UniProt, 2019) as of 2018-12-18. Subcellular locations *Nucleus*, *Nucleus speckle*, *Chromosome*, *Nucleus matrix*, *Nucleus envelope*, *Nucleus inner membrane*, *Nucleus membrane*, *Nucleus outer membrane* were treated as nuclear. Proteins with no localisation information were assumed to be nuclear. Non-nuclear proteins were discarded. Intensities (either SILAC-labelled or LFQ) of the remaining proteins were

15 normalised using TMM (Robinson and Oshlack, 2010). For SILAC experiments, log2 protein intensities were converted into log2(H/L) ratios which were compared between forward and reverse experiments. Outlier proteins that did not show typical anticorrelation between forward and reverse H/L ratio in SILAC experiments were detected and removed by estimating the direction of first and second principal components of pooled ratios of significantly enriched

20 proteins in all experiments (forward log2 ratio >1.25, reverse <-1.25 or vice-versa) and discarding all proteins 2.5-standard deviations away from the median in the second principal direction. This procedure was been performed twice, adjusting the PCA estimates once more after removing outlier proteins. Intensities of remaining proteins were re-normalised again using TMM. The ratio outlier filtering step was skipped in LFQ dataset.

25

Normalised intensities of remaining proteins were analysed using Limma (Kammers et al., 2015; Ritchie et al., 2015). Three and nine-hour Pol II inhibition datasets were analysed separately, as were RNase-treated chromatin and nucleosome affinity purification experiments. SILAC experiments were modelled based on the log2 intensities of proteins, assuming additive treatment (inhibitor vs DMSO or RNase vs Mock) effect, additive mix (SILAC experiment batch) bias, and additive isotope (H/L labelling) bias. The change of intensity after washout of flavopiridol (relative to intensity after 3 hr flavopiridol treatment) was modelled as an additional parameter in three-hour inhibition model. The change of intensity after addition of tRNA (as compared to RNase treatment without tRNA) was modelled similarly in SILAC nucleosome purification experiments. The label-free chromatin RNase treatment dataset was modelled assuming additive treatment effect (RNase vs Mock) and paired experiment batch effects. Limma models were fitted with trend parameter set. Statistical testing was performed on treatment and washout/tRNA terms. P-values were adjusted by Benjamini/Hochberg method, significance was assumed at FDR of 0.05. Comparisons between the different experiments were performed by matching the outputs by UniProt protein IDs, discarding rows that map ambiguously. To allow direct comparison to the Pol II inhibition data, only proteins with UniProt protein IDs that were also present in the RNA pol II inhibition dataset were visualised in the RNaseA treatment volcano plots and FDR values were calculated based on the population of proteins that were also detected in the RNA Pol II inhibition experiment.

We identified proteins that were significantly enriched or depleted in the chromatin fraction upon treatment with both flavopiridol and triptolide at 9 hrs (FDR<0.05). To measure the effect of flavopiridol washout, we identified all proteins significantly enriched or depleted on chromatin after 3 hours incubation (FDR<0.05) that were also detected in the washout experiment (n=523). We then calculated the Pearson correlation between log2(FP 3hr/DMSO

41

3hr and log2(washout/FP3hr) and its significance (corr.test in R, which applies a t-test). We also identified proteins significantly enriched or depleted in the chromatin fraction after RNaseA treatment (FDR<0.05) and proteins with significantly increased or decreased binding to nucleosomes after RNA degradation (FDR<0.05). We took the set of proteins significantly enriched or depleted in the chromatin fraction upon treatment with both flavopiridol and triptolide at 9 hrs and calculated the average change in chromatin binding between the two treatments. We then calculated the correlation between these values and the change in chromatin binding caused by RNaseA treatment. The significance of correlations between datasets was estimated using corr.test in R. The significance of overlaps between sets of proteins depleted or enriched on chromatin after Pol II inhibition and RNaseA treatment were compared using the hypergeometric test in R using the set of proteins detected in both treatments as the population.

Gene names were reannotated using the Mouse Genome Informatics (MGI) database and used to perform enrichment analysis against the GO (release 2020-01-01), Reactome (2020-2-7), KEGG (2020-02-03) and WP (20200110) databases using the hypergeometric test in g:Profiler2 v1.2 (Raudvere et al., 2019). Mouse proteins annotated with the terms RNA processing (GO:0006396) or Chromatin organisation (GO:0006325) were downloaded from AmiGO 2 (http://amigo.geneontology.org/amigo) and used to identify proteins with these functions in the volcano plots. Mouse gene names were also mapped to human gene names using Ensembl BioMart (http://www.ensembl.org/biomart/martview/). Mouse gene names that did not match any human gene names using BioMart were checked using HGNC multi-symbol checker (https://www.genenames.org/tools/multi-symbol-checker/) and then mapped to their human gene names. Protein complexes with significant enrichment of subunits in the set of recruited or depleted proteins were identified from CORUM 3.0 (03.09.2018) (Giurgiu et al.,

2019) using the hypergeometric test in g:profiler2 v1.2. Subunits missing from CORUM were manually added to the cytoscape figures and a hypergeometric test repeated to ensure the complexes remained significant. Additional complexes or functionally related groups not annotated in CORUM were also added if significant (these were DNMTs, EHMTs, HUSH, NoRC, P-TEFb, SEC and SAFB factors in Figure 1C and PRC1.6 and NSL in Figure 3C). Complexes were depicted using Cytoscape v3.5 (Shannon et al., 2003). Interactions between proteins in these complexes was taken from STRING v11 (Szklarczyk et al., 2019) using experiments as the active interaction source.

iCLIP data analysis

iCLIP data were processed using iCount (https://github.com/tomazc/iCount) as described (Beltran et al., 2019). The unique molecular identifiers (UMIs) were registered and experimental barcodes removed before mapping the sequences to mm9 using Bowtie version 0.12.7 (command line: -v 2 -m 1 -a --best --strata) in iCount. Reads indicative of PCR duplicates (reads mapping to the same position with the same UMI) and reads aligning to multiple positions in the genome were removed. Data from independent replicate samples were then added together (P-TEFb n=3; LARP7 n=2, Input n=1, P-TEFb in pla-B-treated cells n=1, P-TEFb in DMSO-treated cells n=1). When mapping crosslinks to genes, crosslinks overlapping a RepeatMasker feature or ncRNAs under 200 nt in length or annotated as a snoRNA were removed. Crosslink sites were assigned to the nearest splice site junction by iCount (Ensembl59 annotation). First exon-intron, mid exon-intron, intron- mid exon and last intron-exon junctions were defined as those uniquely annotated with these designations by Ensembl59. The number of crosslink sites at each position were normalized by the total number of exons or introns at that position and by the total number of crosslink sites in the dataset multiplied by 10^9. The data points were smoothened over a 12-nt sliding window using the

smth.gaussian function from the smoother package in R with smoother.gaussianwindow.alpha = 2.3 and plotted with the ggplot2 package in R. We used MISO (Katz et al., 2010) to identify included exons (posterior mean value > 0.90) and excluded exons (posterior mean value < 0.10) from previously published mESC mRNA-seq data (Beltran et al., 2016). Exon-intron junctions that were also annotated in Ensembl 59 were retained and P-TEFb and input crosslinks over the exon-intron boundaries were normalized, smoothened and plotted as above. When plotting RNA crosslinking at individual genes, high-confidence clusters of crosslink sites were identified using the low FDR function in iCount (FDR<0.05), with a 50 nt flank (Konig et al., 2010).

For comparison of P-TEFb RNA crosslinking at single-exon versus multi-exon genes, exon number was identified from the Ensembl 59 annotation. The number of P-TEFb and input RNA crosslinks per gene were normalized by the total number of reads mapping to all the genes and multiplied by a factor of 1 million. For genes with crosslinks in both samples, the log2 ratios (P-TEFb/input) were plotted and a t-test performed.

For mapping crosslinks to 7SK and snRNAs, non-transcribed 7SK pseudogenes were masked in the mm9 genome sequence and reads aligned using bowtie2 version 2.1.0 (command line parameters: --very-sensitive --no-unal) (Langmead and Salzberg, 2012). Reads aligning to multiple positions in the genome were removed, but for this analysis, reads mapping to the same position with the same UMI were retained due to the risk of high abundance target RNAs saturating the number of possible UMIs (4^5).

RNA-seq analysis

RNA-Seq data were aligned to concatenated mouse-drosophila genome (mm9 and BDGP5.25 assembly) using STAR (version 2.7.3a) (Dobin et al., 2013). Uniquely mapped reads were extracted from the aligned bam files, which were then split into Mouse and Drosophila. The number of reads mapping to the Drosophila genome were used to calculate a scaling factor that

5   was then used to scale the Mouse bigwig files generated using deepTools (version 3.0.2) (Ramirez et al., 2016). Exonic and intronic coordinates were extracted from Ensembl 67 annotation and featureCounts (Liao et al., 2014) in R used to count the number of reads in exons or introns for each Mouse gene. The number of reads mapping to a gene in Drosophila was counted by featureCounts using a gtf file (version 5.25). DESeq2 (Love et al., 2014) was

10   used to calculate the size-factors for the Drosophila reads and these were then used to normalize the read counts mapping to the Mouse genome. A pseudo-count of 1 was added to the data and log2 ratios calculated relative to t=0 (for Pol II inhibition) or mock (for RNaseA). Gene biotype information was downloaded for Ensembl 67 using BioMart (Smedley et al., 2009). Genes with a non-coding biotype were assigned to lincRNA biotype after manual curation. Cumulative

15   frequency distribution plots were generated from log2 ratios using ggplot2 (Wickham, 2016). Metagene plots were generated using the computeMatrix and plotProfile functions in deepTools.

20   **Comparison to RNA binding studies**

Table S1 indicating whether proteins were detected in previously published RNA binding studies was downloaded from (Caudron-Herger et al., 2019) and the data compared to our data using human protein names. Proteins that increase on chromatin upon both 9hrs TRP and FP treatment (FDR<0.05), proteins that decrease on chromatin upon both 9hrs TRP and FP

25   treatment (FDR<0.05) and proteins remaining constant on chromatin upon both 9hrs TRP and FP treatment (FDR>0.05) were identified and the proportion of proteins in each of these sets

identified to bind RNA in each study was quantified. The significance of the proportion of proteins that increase and decrease on chromatin identified as RNA binding proteins was estimated relative the proportion of non-changing proteins identified as RNA binding proteins using the Binomial test and the p-values adjusted for multiple hypothesis testing to reflect the 12 studies assessed.

CLIP and immunoblotting

P-TEFb (n=7) and LARP7 (n=2) RNA crosslinking was quantified in cells treated with 7SK ASO relative to RNA crosslinking in cells treated with scrambled ASO and normalised to change in CyclinT1 or LARP7 protein amount. The mean and S.D of these values were then plotted and the significance of the change in RNA crosslinking (7SK/scrambled) estimated using a 1-sided Welch's unequal variance t-test.

CyclinT1, CDK9, LARP7 and SMARCC1 chromatin binding was quantified 3 or 6 hrs after treatment with triptolide relative to before treatment in the same cell line in triplicate and the mean and S.D. plotted. The significance of the difference between WT and KO cells at the same timepoint was estimated using a 1-sided Student's t-test.

SUPPLEMENTARY INFORMATION

Table S1. Changes in the association of proteins with chromatin after Pol II inhibition.
Related to Figure 1.

5

Table S2. Enriched functional categories in the set of proteins whose association with chromatin is regulated by transcription.
Related to Figure 1.

10 **Table S3. Changes in the association of proteins with chromatin after RNA degradation. q-values (FDR) calculated using all detected proteins and calculated using the set of proteins also detected in the Pol II inhibition experiment are included.**
Related to Figure 2.

15 **Table S4. Enriched functional categories in the set of proteins whose association with chromatin is regulated by RNA.**
Related to Figure 2.

Table S5. Changes in binding of proteins to nucleosomes after RNA degradation in
20 **nuclear extract.**
Related to Figure 3.

Table S6. Enriched functional categories in the set of proteins whose association with nucleosomes is regulated by RNA.
25 Related to Figure 3.

REFERENCES

Bacon, C.W., and D'Orso, I. (2019). CDK9: a signaling hub for transcriptional control. Transcription *10*, 57-75.

Baillat, D., Hakimi, M.A., Naar, A.M., Shilatifard, A., Cooch, N., and Shiekhattar, R. (2005). Integrator, a multiprotein mediator of small nuclear RNA processing, associates with the C-terminal repeat of RNA polymerase II. Cell *123*, 265-276.

Baltz, A.G., Munschauer, M., Schwanhausser, B., Vasile, A., Murakawa, Y., Schueler, M., Youngs, N., Penfold-Brown, D., Drew, K., Milek, M.*, et al.* (2012). The mRNA-bound proteome and its global occupancy profile on protein-coding transcripts. Mol Cell *46*, 674-690.

Bao, X., Guo, X., Yin, M., Tariq, M., Lai, Y., Kanwal, S., Zhou, J., Li, N., Lv, Y., Pulido-Quetglas, C.*, et al.* (2018). Capturing the interactome of newly transcribed RNA. Nat Methods *15*, 213-220.

Barboric, M., Yik, J.H., Czudnochowski, N., Yang, Z., Chen, R., Contreras, X., Geyer, M., Matija Peterlin, B., and Zhou, Q. (2007). Tat competes with HEXIM1 to increase the active pool of P-TEFb for HIV-1 transcription. Nucleic Acids Res *35*, 2003-2012.

Barutcu, A.R., Blencowe, B.J., and Rinn, J.L. (2019). Differential contribution of steady-state RNA and active transcription in chromatin organization. EMBO Rep *20*, e48068.

Battaglia, S., Lidschreiber, M., Baejen, C., Torkler, P., Vos, S.M., and Cramer, P. (2017). RNA-dependent chromatin association of transcription elongation factors and Pol II CTD kinases. Elife *6*.

Beckmann, B.M., Horos, R., Fischer, B., Castello, A., Eichelbaum, K., Alleaume, A.M., Schwarzl, T., Curk, T., Foehr, S., Huber, W.*, et al.* (2015). The RNA-binding proteomes from yeast to man harbour conserved enigmRBPs. Nat Commun *6*, 10127.

Beltran, M., Tavares, M., Justin, N., Khandelwal, G., Ambrose, J., Foster, B.M., Worlock, K.B., Tvardovskiy, A., Kunzelmann, S., Herrero, J.*, et al.* (2019). G-tract RNA removes Polycomb repressive complex 2 from genes. Nat Struct Mol Biol *26*, 899-909.

Beltran, M., Yates, C.M., Skalska, L., Dawson, M., Reis, F.P., Viiri, K., Fisher, C.L., Sibley, C.R., Foster, B.M., Bartke, T.*, et al.* (2016). The interaction of PRC2 with RNA or chromatin is mutually antagonistic. Genome Res *26*, 896-907.

Bi, X., Xu, Y., Li, T., Li, X., Li, W., Shao, W., Wang, K., Zhan, G., Wu, Z., Liu, W.*, et al.* (2019). RNA Targets Ribogenesis Factor WDR43 to Chromatin for Transcription and Pluripotency Control. Mol Cell *75*, 102-116 e109.

Bugai, A., Quaresma, A.J.C., Friedel, C.C., Lenasi, T., Duster, R., Sibley, C.R., Fujinaga, K., Kukanja, P., Hennig, T., Blasius, M.*, et al.* (2019). P-TEFb Activation by RBM7 Shapes a Pro-survival Transcriptional Response to Genotoxic Stress. Mol Cell *74*, 254-267 e210.

Caizzi, L., Monteiro-Martins, S., Schwalb, B., Lysakovskaia, K., Schmitzova, J., Sawicka, A., Chen, Y., Lidschreiber, M., and Cramer, P. (2021). Efficient RNA polymerase II pause release requires U2 snRNP function. Mol Cell. https://doi.org/10.1016/j.molcel.2021.02.016

Cajigas, I., Leib, D.E., Cochrane, J., Luo, H., Swyter, K.R., Chen, S., Clark, B.S., Thompson, J., Yates, J.R., 3rd, Kingston, R.E.*, et al.* (2015). Evf2 lncRNA/BRG1/DLX1 interactions reveal RNA-dependent inhibition of chromatin remodeling. Development *142*, 2641-2652.

Calo, E., Flynn, R.A., Martin, L., Spitale, R.C., Chang, H.Y., and Wysocka, J. (2015). RNA helicase DDX21 coordinates transcription and ribosomal RNA processing. Nature *518*, 249-253.

Castello, A., Fischer, B., Eichelbaum, K., Horos, R., Beckmann, B.M., Strein, C., Davey, N.E., Humphreys, D.T., Preiss, T., Steinmetz, L.M.*, et al.* (2012). Insights into RNA biology from an atlas of mammalian mRNA-binding proteins. Cell *149*, 1393-1406.

Castello, A., Fischer, B., Frese, C.K., Horos, R., Alleaume, A.M., Foehr, S., Curk, T., Krijgsveld, J., and Hentze, M.W. (2016). Comprehensive Identification of RNA-Binding Domains in Human Cells. Mol Cell *63*, 696-710.

Caudron-Herger, M., Rusin, S.F., Adamo, M.E., Seiler, J., Schmid, V.K., Barreau, E., Kettenbach, A.N., and Diederichs, S. (2019). R-DeeP: Proteome-wide and Quantitative Identification of RNA-Dependent Proteins by Density Gradient Ultracentrifugation. Mol Cell *75*, 184-199 e110.

Chathoth, K.T., Barrass, J.D., Webb, S., and Beggs, J.D. (2014). A splicing-dependent transcriptional checkpoint associated with prespliceosome formation. Mol Cell *53*, 779-790.

Chen, K., Hu, J., Moore, D.L., Liu, R., Kessans, S.A., Breslin, K., Lucet, I.S., Keniry, A., Leong, H.S., Parish, C.L.*, et al.* (2015). Genome-wide binding and mechanistic analyses of Smchd1-mediated epigenetic regulation. Proc Natl Acad Sci U S A *112*, E3535-3544.

Cifuentes-Rojas, C., Hernandez, A.J., Sarma, K., and Lee, J.T. (2014). Regulatory interactions between RNA and polycomb repressive complex 2. Mol Cell *55*, 171-185.

Conrad, T., Albrecht, A.S., de Melo Costa, V.R., Sauer, S., Meierhofer, D., and Orom, U.A. (2016). Serial interactome capture of the human cell nucleus. Nat Commun *7*, 11212.

Cox, J., and Mann, M. (2008). MaxQuant enables high peptide identification rates, individualized p.p.b.-range mass accuracies and proteome-wide protein quantification. Nat Biotechnol *26*, 1367-1372.

D'Orso, I., and Frankel, A.D. (2010). RNA-mediated displacement of an inhibitory snRNP complex activates transcription elongation. Nat Struct Mol Biol *17*, 815-821.

Davidovic, L., Bechara, E., Gravel, M., Jaglin, X.H., Tremblay, S., Sik, A., Bardoni, B., and Khandjian, E.W. (2006). The nuclear microspherule protein 58 is a novel RNA-binding protein that interacts with fragile X mental retardation protein in polyribosomal mRNPs from neurons. Hum Mol Genet *15*, 1525-1538.

Davidovich, C., Zheng, L., Goodrich, K.J., and Cech, T.R. (2013). Promiscuous RNA binding by Polycomb repressive complex 2. Nat Struct Mol Biol *20*, 1250-1257.

Di Ruscio, A., Ebralidze, A.K., Benoukraf, T., Amabile, G., Goff, L.A., Terragni, J., Figueroa, M.E., De Figueiredo Pontes, L.L., Alberich-Jorda, M., Zhang, P.*, et al.* (2013). DNMT1-interacting RNAs block gene-specific DNA methylation. Nature *503*, 371-376.

Dobin, A., Davis, C.A., Schlesinger, F., Drenkow, J., Zaleski, C., Jha, S., Batut, P., Chaisson, M., and Gingeras, T.R. (2013). STAR: ultrafast universal RNA-seq aligner. Bioinformatics *29*, 15-21.

Flynn, R.A., Do, B.T., Rubin, A.J., Calo, E., Lee, B., Kuchelmeister, H., Rale, M., Chu, C., Kool, E.T., Wysocka, J.*, et al.* (2016). 7SK-BAF axis controls pervasive transcription at enhancers. Nat Struct Mol Biol *23*, 231-238.

Fong, Y.W., and Zhou, Q. (2001). Stimulatory effect of splicing factors on transcriptional elongation. Nature *414*, 929-933.

Garber, M.E., Wei, P., KewalRamani, V.N., Mayall, T.P., Herrmann, C.H., Rice, A.P., Littman, D.R., and Jones, K.A. (1998). The interaction between HIV-1 Tat and human cyclin T1 requires zinc and a critical cysteine residue that is not conserved in the murine CycT1 protein. Genes Dev *12*, 3512-3527.

Garland, W., Comet, I., Wu, M., Radzisheuskaya, A., Rib, L., Vitting-Seerup, K., Lloret-Llinares, M., Sandelin, A., Helin, K., and Jensen, T.H. (2019). A Functional Link between Nuclear RNA Decay and Transcriptional Control Mediated by the Polycomb Repressive Complex 2. Cell Rep *29*, 1800-1811 e1806.

Giurgiu, M., Reinhard, J., Brauner, B., Dunger-Kaltenbach, I., Fobo, G., Frishman, G., Montrone, C., and Ruepp, A. (2019). CORUM: the comprehensive resource of mammalian protein complexes-2019. Nucleic Acids Res *47*, D559-D563.

Han, P., Li, W., Lin, C.H., Yang, J., Shang, C., Nuernberg, S.T., Jin, K.K., Xu, W., Lin, C.Y., Lin, C.J.*, et al.* (2014). A long noncoding RNA protects the heart from pathological hypertrophy. Nature *514*, 102-106.

Hansen, A.S., Hsieh, T.S., Cattoglio, C., Pustova, I., Saldana-Meyer, R., Reinberg, D., Darzacq, X., and Tjian, R. (2019). Distinct Classes of Chromatin Loops Revealed by Deletion of an RNA-Binding Region in CTCF. Mol Cell *76*, 395-411 e313.

He, C., Sidoli, S., Warneford-Thomson, R., Tatomer, D.C., Wilusz, J.E., Garcia, B.A., and Bonasio, R. (2016). High-Resolution Mapping of RNA-Binding Regions in the Nuclear Proteome of Embryonic Stem Cells. Mol Cell *64*, 416-430.

Heinz, S., Texari, L., Hayes, M.G.B., Urbanowski, M., Chang, M.W., Givarkes, N., Rialdi, A., White, K.M., Albrecht, R.A., Pache, L.*, et al.* (2018). Transcription Elongation Can Affect Genome 3D Structure. Cell *174*, 1522-1536 e1522.

Hendrickson, D.G., Kelley, D.R., Tenen, D., Bernstein, B., and Rinn, J.L. (2016). Widespread RNA binding by chromatin-associated proteins. Genome Biol *17*, 28.

Herzel, L., Ottoz, D.S.M., Alpert, T., and Neugebauer, K.M. (2017). Splicing and transcription touch base: co-transcriptional spliceosome assembly and function. Nat Rev Mol Cell Biol *18*, 637-650.

Herzog, V.A., Lempradl, A., Trupke, J., Okulski, H., Altmutter, C., Ruge, F., Boidol, B., Kubicek, S., Schmauss, G., Aumayr, K.*, et al.* (2014). A strand-specific switch in noncoding transcription switches the function of a Polycomb/Trithorax response element. Nat Genet *46*, 973-981.

Hnisz, D., Shrinivas, K., Young, R.A., Chakraborty, A.K., and Sharp, P.A. (2017). A Phase Separation Model for Transcriptional Control. Cell *169*, 13-23.

Hooper, M., Hardy, K., Handyside, A., Hunter, S., and Monk, M. (1987). HPRT-deficient (Lesch-Nyhan) mouse embryos derived from germline colonization by cultured cells. Nature *326*, 292-295.

Hosogane, M., Funayama, R., Shirota, M., and Nakayama, K. (2016). Lack of Transcription Triggers H3K27me3 Accumulation in the Gene Body. Cell Rep *16*, 696-706.

Hu, Y.W., Guo, F.X., Xu, Y.J., Li, P., Lu, Z.F., McVey, D.G., Zheng, L., Wang, Q., Ye, J.H., Kang, C.M.*, et al.* (2019). Long noncoding RNA NEXN-AS1 mitigates atherosclerosis by regulating the actin-binding protein NEXN. J Clin Invest *129*, 1115-1128.

Huppertz, I., Attig, J., D'Ambrogio, A., Easton, L.E., Sibley, C.R., Sugimoto, Y., Tajnik, M., Konig, J., and Ule, J. (2014). iCLIP: protein-RNA interactions at nucleotide resolution. Methods *65*, 274-287.

Jegu, T., Blum, R., Cochrane, J.C., Yang, L., Wang, C.Y., Gilles, M.E., Colognori, D., Szanto, A., Marr, S.K., Kingston, R.E.*, et al.* (2019). Xist RNA antagonizes the SWI/SNF chromatin remodeler BRG1 on the inactive X chromosome. Nat Struct Mol Biol *26*, 96-109.

Jeon, Y., and Lee, J.T. (2011). YY1 tethers Xist RNA to the inactive X nucleation center. Cell *146*, 119-133.

Ji, X., Zhou, Y., Pandit, S., Huang, J., Li, H., Lin, C.Y., Xiao, R., Burge, C.B., and Fu, X.D. (2013). SR proteins collaborate with 7SK and promoter-associated nascent RNA to release paused polymerase. Cell *153*, 855-868.

Kammers, K., Cole, R.N., Tiengwe, C., and Ruczinski, I. (2015). Detecting Significant Changes in Protein Abundance. EuPA Open Proteom *7*, 11-19.

Kaneko, S., Son, J., Bonasio, R., Shen, S.S., and Reinberg, D. (2014). Nascent RNA interaction keeps PRC2 activity poised and in check. Genes Dev *28*, 1983-1988.

Kaneko, S., Son, J., Shen, S.S., Reinberg, D., and Bonasio, R. (2013). PRC2 binds active promoters and contacts nascent RNAs in embryonic stem cells. Nat Struct Mol Biol *20*, 1258-1264.

Kanhere, A., Viiri, K., Araújo, C.C., Rasaiyaah, J., Bouwman, R.D., Whyte, W.A., Pereira, C.F., Brookes, E., Walker, K., Bell, G.W., *et al.* (2010). Short RNAs are transcribed from repressed Polycomb target genes and interact with Polycomb Repressive Complex-2. Mol Cell *38*, 675-688.

5   Katz, Y., Wang, E.T., Airoldi, E.M., and Burge, C.B. (2010). Analysis and design of RNA sequencing experiments for identifying isoform regulation. Nat Methods *7*, 1009-1015.

Koga, M., Hayashi, M., and Kaida, D. (2015). Splicing inhibition decreases phosphorylation level of Ser2 in Pol II CTD. Nucleic Acids Res *43*, 8258-8267.

Konig, J., Zarnack, K., Rot, G., Curk, T., Kayikci, M., Zupan, B., Turner, D.J., Luscombe, N.M., and Ule, J. (2010). iCLIP reveals the function of hnRNP particles in splicing at individual nucleotide resolution. Nat Struct Mol Biol *17*, 909-915.

10

Kung, J.T., Kesner, B., An, J.Y., Ahn, J.Y., Cifuentes-Rojas, C., Colognori, D., Jeon, Y., Szanto, A., del Rosario, B.C., Pinter, S.F.*, et al.* (2015). Locus-specific targeting to the X chromosome revealed by the RNA interactome of CTCF. Mol Cell *57*, 361-375.

15   Kwon, S.C., Yi, H., Eichelbaum, K., Fohr, S., Fischer, B., You, K.T., Castello, A., Krijgsveld, J., Hentze, M.W., and Kim, V.N. (2013). The RNA-binding protein repertoire of embryonic stem cells. Nat Struct Mol Biol *20*, 1122-1130.

Langmead, B., and Salzberg, S.L. (2012). Fast gapped-read alignment with Bowtie 2. Nat Methods *9*, 357-359.

20   Li, L., Lyu, X., Hou, C., Takenaka, N., Nguyen, H.Q., Ong, C.T., Cubenas-Potts, C., Hu, M., Lei, E.P., Bosco, G.*, et al.* (2015). Widespread rearrangement of 3D chromatin organization underlies polycomb-mediated stress-induced silencing. Mol Cell *58*, 216-231.

Li, W., Notani, D., Ma, Q., Tanasa, B., Nunez, E., Chen, A.Y., Merkurjev, D., Zhang, J., Ohgi, K., Song, X.*, et al.* (2013). Functional roles of enhancer RNAs for oestrogen-dependent 25   transcriptional activation. Nature *498*, 516-520.

Liao, Y., Smyth, G.K., and Shi, W. (2014). featureCounts: an efficient general purpose program for assigning sequence reads to genomic features. Bioinformatics *30*, 923-930.

Lin, S., Coutinho-Mansfield, G., Wang, D., Pandit, S., and Fu, X.D. (2008). The splicing factor SC35 has an active role in transcriptional elongation. Nat Struct Mol Biol *15*, 819-826.

30   Love, M.I., Huber, W., and Anders, S. (2014). Moderated estimation of fold change and dispersion for RNA-seq data with DESeq2. Genome Biol *15*, 550.

Makowski, M.M., Grawe, C., Foster, B.M., Nguyen, N.V., Bartke, T., and Vermeulen, M. (2018). Global profiling of protein-DNA and protein-nucleosome binding affinities using quantitative mass spectrometry. Nat Commun *9*, 1653.

35   Mayer, C., Schmitz, K.M., Li, J., Grummt, I., and Santoro, R. (2006). Intergenic transcripts regulate the epigenetic state of rRNA genes. Mol Cell *22*, 351-361.

McNamara, R.P., Reeder, J.E., McMillan, E.A., Bacon, C.W., McCann, J.L., and D'Orso, I. (2016). KAP1 Recruitment of the 7SK snRNP Complex to Promoters Enables Transcription Elongation by RNA Polymerase II. Mol Cell *61*, 39-53.

Michels, A.A., Nguyen, V.T., Fraldi, A., Labas, V., Edwards, M., Bonnet, F., Lania, L., and Bensaude, O. (2003). MAQ1 and 7SK RNA interact with CDK9/cyclin T complexes in a transcription-dependent manner. Mol Cell Biol *23*, 4859-4869.

Mondal, T., Rasmussen, M., Pandey, G.K., Isaksson, A., and Kanduri, C. (2010). Characterization of the RNA content of chromatin. Genome Res *20*, 899-907.

Monte, E., Chen, H., Kolmakova, M., Parvatiyar, M., Vondriska, T.M., and Franklin, S. (2012). Quantitative analysis of chromatin proteomes in disease. J Vis Exp. *70*, 4294

Mullari, M., Lyon, D., Jensen, L.J., and Nielsen, M.L. (2017). Specifying RNA-Binding Regions in Proteins by Peptide Cross-Linking and Affinity Purification. J Proteome Res *16*, 2762-2772.

Nickerson, J.A., Krochmalnic, G., Wan, K.M., and Penman, S. (1989). Chromatin architecture and nuclear RNA. Proc Natl Acad Sci U S A *86*, 177-181.

Nozawa, R.S., Boteva, L., Soares, D.C., Naughton, C., Dun, A.R., Buckle, A., Ramsahoye, B., Bruton, P.C., Saleeb, R.S., Arnedo, M.*, et al.* (2017). SAF-A Regulates Interphase Chromosome Structure through Oligomerization with Chromatin-Associated RNAs. Cell *169*, 1214-1227 e1218.

Nozawa, R.S., and Gilbert, N. (2019). RNA: Nuclear Glue for Folding the Genome. Trends Cell Biol *29*, 201-211.

Pan, H., Jin, M., Ghadiyaram, A., Kaur, P., Miller, H.E., Ta, H.M., Liu, M., Fan, Y., Mahn, C., Gorthi, A.*, et al.* (2020). Cohesin SA1 and SA2 are RNA binding proteins that localize to RNA containing regions on DNA. Nucleic Acids Res. *48*, 5639-565.

Perez-Perri, J.I., Rogell, B., Schwarzl, T., Stein, F., Zhou, Y., Rettel, M., Brosig, A., and Hentze, M.W. (2018). Discovery of RNA-binding proteins and characterization of their dynamic responses by enhanced RNA interactome capture. Nat Commun *9*, 4408.

Perez-Riverol, Y., Csordas, A., Bai, J., Bernal-Llinares, M., Hewapathirana, S., Kundu, D.J., Inuganti, A., Griss, J., Mayer, G., Eisenacher, M.*, et al.* (2019). The PRIDE database and related tools and resources in 2019: improving support for quantification data. Nucleic Acids Res *47*, D442-D450.

Prensner, J.R., Iyer, M.K., Sahu, A., Asangani, I.A., Cao, Q., Patel, L., Vergara, I.A., Davicioni, E., Erho, N., Ghadessi, M.*, et al.* (2013). The long noncoding RNA SChLAP1 promotes aggressive prostate cancer and antagonizes the SWI/SNF complex. Nat Genet *45*, 1392-1398.

Quaresma, A., Bugai, A., and Barboric, M. (2016). Cracking the control of RNA polymerase II elongation by 7SK snRNP and P-TEFb. Nucleic Acids Res *44*, 7527-7539.

Rahnamoun, H., Lee, J., Sun, Z., Lu, H., Ramsey, K.M., Komives, E.A., and Lauberth, S.M. (2018). RNAs interact with BRD4 to promote enhanced chromatin engagement and transcription activation. Nat Struct Mol Biol *25*, 687-697.

Ramirez, F., Ryan, D.P., Gruning, B., Bhardwaj, V., Kilpert, F., Richter, A.S., Heyne, S., Dundar, F., and Manke, T. (2016). deepTools2: a next generation web server for deep-sequencing data analysis. Nucleic Acids Res *44*, W160-165.

Raudvere, U., Kolberg, L., Kuzmin, I., Arak, T., Adler, P., Peterson, H., and Vilo, J. (2019). g:Profiler: a web server for functional enrichment analysis and conversions of gene lists (2019 update). Nucleic Acids Res *47*, W191-W198.

Reynolds, N., Salmon-Divon, M., Dvinge, H., Hynes-Allen, A., Balasooriya, G., Leaford, D., Behrens, A., Bertone, P., and Hendrich, B. (2012). NuRD-mediated deacetylation of H3K27 facilitates recruitment of Polycomb Repressive Complex 2 to direct gene repression. EMBO J *31*, 593-605.

Richter, S., Ping, Y.H., and Rana, T.M. (2002). TAR RNA loop: a scaffold for the assembly of a regulatory switch in HIV replication. Proc Natl Acad Sci U S A *99*, 7928-7933.

Riising, E.M., Comet, I., Leblanc, B., Wu, X., Johansen, J.V., and Helin, K. (2014). Gene silencing triggers polycomb repressive complex 2 recruitment to CpG islands genome wide. Mol Cell *55*, 347-360.

Rinn, J.L., and Chang, H.Y. (2012). Genome regulation by long noncoding RNAs. Annu Rev Biochem *81*, 145-166.

Ritchie, M.E., Phipson, B., Wu, D., Hu, Y., Law, C.W., Shi, W., and Smyth, G.K. (2015). limma powers differential expression analyses for RNA-sequencing and microarray studies. Nucleic Acids Res *43*, e47.

Rivers, C., Idris, J., Scott, H., Rogers, M., Lee, Y.B., Gaunt, J., Phylactou, L., Curk, T., Campbell, C., Ule, J.*, et al.* (2015). iCLIP identifies novel roles for SAFB1 in regulating RNA processing and neuronal function. BMC Biol *13*, 111.

Robinson, M.D., and Oshlack, A. (2010). A scaling normalization method for differential expression analysis of RNA-seq data. Genome Biol *11*, R25.

Saldana-Meyer, R., Gonzalez-Buendia, E., Guerrero, G., Narendra, V., Bonasio, R., Recillas-Targa, F., and Reinberg, D. (2014). CTCF regulates the human p53 gene through direct interaction with its natural antisense transcript, Wrap53. Genes Dev *28*, 723-734.

Saldana-Meyer, R., Rodriguez-Hernaez, J., Escobar, T., Nishana, M., Jacome-Lopez, K., Nora, E.P., Bruneau, B.G., Tsirigos, A., Furlan-Magaril, M., Skok, J.*, et al.* (2019). RNA Interactions Are Essential for CTCF-Mediated Genome Organization. Mol Cell *76*, 412-422 e415.

Savell, K.E., Gallus, N.V., Simon, R.C., Brown, J.A., Revanna, J.S., Osborn, M.K., Song, E.Y., O'Malley, J.J., Stackhouse, C.T., Norvil, A.*, et al.* (2016). Extra-coding RNAs regulate neuronal DNA methylation dynamics. Nat Commun *7*, 12091.

Sedore, S.C., Byers, S.A., Biglione, S., Price, J.P., Maury, W.J., and Price, D.H. (2007). Manipulation of P-TEFb control machinery by HIV: recruitment of P-TEFb from the large form by Tat and binding of HEXIM1 to TAR. Nucleic Acids Res *35*, 4347-4358.

Shannon, P., Markiel, A., Ozier, O., Baliga, N.S., Wang, J.T., Ramage, D., Amin, N., Schwikowski, B., and Ideker, T. (2003). Cytoscape: a software environment for integrated models of biomolecular interaction networks. Genome Res *13*, 2498-2504.

Sigova, A.A., Abraham, B.J., Ji, X., Molinie, B., Hannett, N.M., Guo, Y.E., Jangi, M., Giallourakis, C.C., Sharp, P.A., and Young, R.A. (2015). Transcription factor trapping by RNA in gene regulatory elements. Science *350*, 978-981.

Skalska, L., Beltran-Nebot, M., Ule, J., and Jenner, R.G. (2017). Regulatory feedback from nascent RNA to chromatin and transcription. Nat Rev Mol Cell Biol *18*, 331-337.

Smedley, D., Haider, S., Ballester, B., Holland, R., London, D., Thorisson, G., and Kasprzyk, A. (2009). BioMart--biological queries made easy. BMC Genomics *10*, 22.

St Laurent, G., Shtokalo, D., Tackett, M.R., Yang, Z., Eremina, T., Wahlestedt, C., Urcuqui-Inchima, S., Seilheimer, B., McCaffrey, T.A., and Kapranov, P. (2012). Intronic RNAs constitute the major fraction of the non-coding RNA in mammalian cells. BMC Genomics *13*, 504.

Stock, J.K., Giadrossi, S., Casanova, M., Brookes, E., Vidal, M., Koseki, H., Brockdorff, N., Fisher, A.G., and Pombo A. (2007). Ring1-mediated ubiquitination of H2A restrains poised RNA polymerase II at bivalent genes in mouse ES cells. Nat Cell Biol *9*, 1428-1435.

Studniarek, C., Tellier, M., Martin, P.G.P., Murphy, S., Kiss, T., and Egloff, S. (2021). The 7SK/P-TEFb snRNP controls ultraviolet radiation-induced transcriptional reprogramming. Cell Rep. https://doi.org/10.1016/j.celrep.2021.108965

Szklarczyk, D., Gable, A.L., Lyon, D., Junge, A., Wyder, S., Huerta-Cepas, J., Simonovic, M., Doncheva, N.T., Morris, J.H., Bork, P.*, et al.* (2019). STRING v11: protein-protein association networks with increased coverage, supporting functional discovery in genome-wide experimental datasets. Nucleic Acids Res *47*, D607-D613.

Tie, C.H., Fernandes, L., Conde, L., Robbez-Masson, L., Sumner, R.P., Peacock, T., Rodriguez-Plata, M.T., Mickute, G., Gifford, R., Towers, G.J.*, et al.* (2018). KAP1 regulates endogenous retroviruses in adult human cells and contributes to innate immune control. EMBO Rep *19*.

Trendel, J., Schwarzl, T., Horos, R., Prakash, A., Bateman, A., Hentze, M.W., and Krijgsveld, J. (2019). The Human RNA-Binding Proteome and Its Dynamics during Translational Arrest. Cell *176*, 391-403 e319.

Tsai, P.F., Dell'Orso, S., Rodriguez, J., Vivanco, K.O., Ko, K.D., Jiang, K., Juan, A.H., Sarshad, A.A., Vian, L., Tran, M.*, et al.* (2018). A Muscle-Specific Enhancer RNA Mediates Cohesin Recruitment and Regulates Transcription In trans. Mol Cell *71*, 129-141 e128.

UniProt, C. (2019). UniProt: a worldwide hub of protein knowledge. Nucleic Acids Res *47*, D506-D515.

Wang, K.C., Yang, Y.W., Liu, B., Sanyal, A., Corces-Zimmerman, R., Chen, Y., Lajoie, B.R., Protacio, A., Flynn, R.A., Gupta, R.A.*, et al.* (2011). A long noncoding RNA maintains active chromatin to coordinate homeotic gene expression. Nature *472*, 120-124.

Wang, X., Goodrich, K.J., Gooding, A.R., Naeem, H., Archer, S., Paucek, R.D., Youmans, D.T., Cech, T.R., and Davidovich, C. (2017a). Targeting of Polycomb Repressive Complex 2 to RNA by Short Repeats of Consecutive Guanines. Mol Cell *65*, 1056-1067 e1055.

Wang, X., Paucek, R.D., Gooding, A.R., Brown, Z.Z., Ge, E.J., Muir, T.W., and Cech, T.R. (2017b). Molecular analysis of PRC2 recruitment to DNA in chromatin and its inhibition by RNA. Nat Struct Mol Biol *24*, 1028-1038.

Wei, P., Garber, M.E., Fang, S.M., Fischer, W.H., and Jones, K.A. (1998). A novel CDK9-associated C-type cyclin interacts directly with HIV-1 Tat and mediates its high-affinity, loop-specific binding to TAR RNA. Cell *92*, 451-462.

Werner, M.S., and Ruthenburg, A.J. (2015). Nuclear Fractionation Reveals Thousands of Chromatin-Tethered Noncoding RNAs Adjacent to Active Genes. Cell Rep *12*, 1089-1098.

Wickham, H. (2016). ggplot2: Elegant Graphics for Data Analysis (Springer).

Xue, Y., Pradhan, S.K., Sun, F., Chronis, C., Tran, N., Su, T., Van, C., Vashisht, A., Wohlschlegel, J., Peterson, C.L.*, et al.* (2017). Mot1, Ino80C, and NC2 Function Coordinately to Regulate Pervasive Transcription in Yeast and Mammals. Mol Cell *67*, 594-607 e594.

Yik, J.H., Chen, R., Nishimura, R., Jennings, J.L., Link, A.J., and Zhou, Q. (2003). Inhibition of P-TEFb (CDK9/Cyclin T) kinase and RNA polymerase II transcription by the coordinated actions of HEXIM1 and 7SK snRNA. Mol Cell *12*, 971-982.

Zhang, Q., McKenzie, N.J., Warneford-Thomson, R., Gail, E.H., Flanigan, S.F., Owen, B.M., Lauman, R., Levina, V., Garcia, B.A., Schittenhelm, R.B.*, et al.* (2019). RNA exploits an exposed regulatory site to inhibit the enzymatic activity of PRC2. Nat Struct Mol Biol *26*, 237-247.

Zhao, L., Guo, H., Zhou, B., Feng, J., Li, Y., Han, T., Liu, L., Li, L., Zhang, S., Liu, Y.*, et al.* (2016). Long non-coding RNA SNHG5 suppresses gastric cancer progression by trapping MTA2 in the cytosol. Oncogene *35*, 5770-5780.

Zoabi, M., Nadar-Ponniah, P.T., Khoury-Haddad, H., Usaj, M., Budowski-Tal, I., Haran, T., Henn, A., Mandel-Gutfreund, Y., and Ayoub, N. (2014). RNA-dependent chromatin localization of KDM4D lysine demethylase promotes H3K9me3 demethylation. Nucleic Acids Res *42*, 13026-13038.

Fig 1

a Mock / RNaseA

Chromatin fractionation and LC-MS/MS

b

	Depleted	Recruited
Chromatin organisation	6	50
RNA processing	161	34
Other	57	217

c Depleted / Recruited — Pol II inhibition, RNA degradation

log2 change in chromatin association

d Chromatin modifiers, Nucleosome remodelers, Transcription, Transcription factors, Higher-order structure

e Cyt. Nuc. Chr. WCE

Fig 2

Fig 3

a

3 hrs | 9 hrs

DMSO · TRP | DMSO · FP · Washout | DMSO · FP · TRP

Pol II S2P
Pol II S5P
Pol II total

b

Chromatin-associated introns | WCE polyA+ exons

Protein-coding | lncRNA | Protein-coding | lncRNA

Cumulative frequency distribution

log2FC vs 0 hr

FP 1 hr
FP 3 hr
FP 9 hr

TRP 1 hr
TRP 3 hr
TRP 9 hr

c

Relative signal

-20.0 TSS 100.0

0 hr
FP 1hr
FP 3hr
FP 9hr

0 hr
TRP 1hr
TRP 3hr
TRP 9hr

d

3 hr | 9 hr

H | L | H | L

DMSO TRP FP - FP wash | DMSO TRP FP FP wash | DMSO TRP FP | DMSO TRP FP

250 130 100 70 55 35 25 15 10

e

Cyt. | Nuc. | Chr. | WCE | Time after FP

55 Tubulin
70 SF3A3
15 H3

f

y=0.67x − 0.03
r=0.53, p=8e-108

9hr-Fp, log2 FC / 3hr-Fp, log2 FC

y=0.68x + 0.02
r=0.62, p=4.3e-162

9hr-Trp, log2 FC / 3hr-Trp, log2 FC

y=0.69x − 0.06
r=0.67, p=1.8e-187

3hr-Trp, log2 FC / 3hr-Fp, log2 FC

y=0.60x + 0.02
r=0.66, p=2.9e-196

9hr-Trp, log2 FC / 9hr-Fp, log2 FC

g

Cells (%)

DMSO, FP 3h, FP 9h, TRP 3h, TRP 9h

M
S
G1

h

Dead cells

Cells (%)

DMSO, FP 3h, FP 9h, TRP 3h, TRP 9h, SN-38

Caspase activity

Cells (%)

DMSO, FP 3h, FP 9h, TRP 3h, TRP 9h, SN-38

i

Chromatin | WCE

FP TRP Doxo | FP TRP Doxo

0 3 9 3 9 3 | 0 3 9 3 9 3 Time (hr)

15 γH2A.X
15 H3

j

10 | 1 μM

0 1 3 6 | 6 Time after FP (hr)

250 CHD4
130 DNMT3A
130 SMARCC1
250 INO80
130 STAG1
100 CCNT1
35 CDK9
55 ZFP57
55 UTF1
70 SF3A3
15 H3

k

GO:0005681 spliceosomal complex
GO:0003723 RNA binding
GO:0006396 RNA processing
GO:0006325 chromatin organization
GO:0006351 transcription, DNA-templated
GO:0051276 chromosome organization
GO:0003682 chromatin binding
WP:WP1763 PluriNetWork

-log10 p-value

Recruited to chromatin
Depleted from chromatin

l

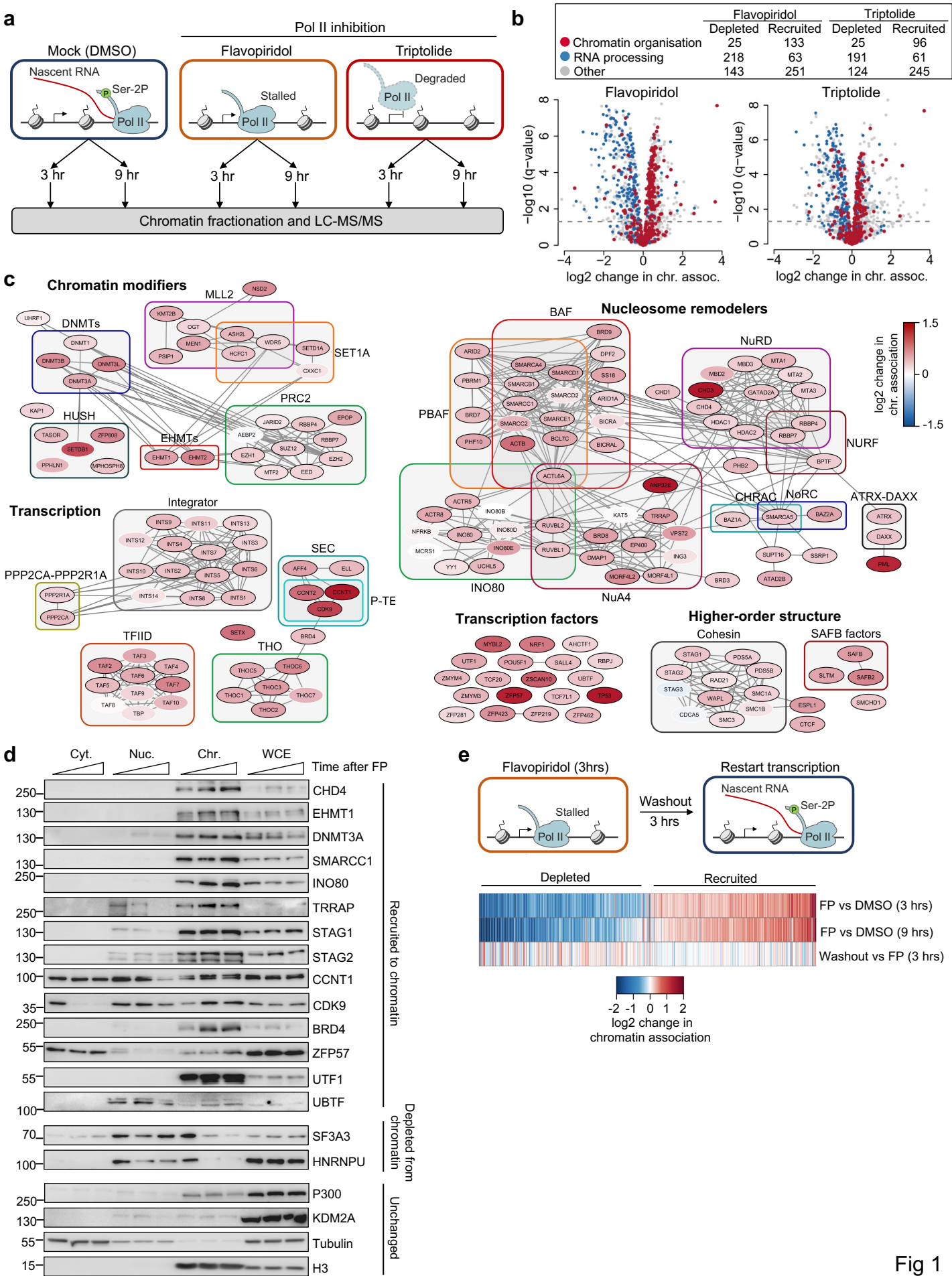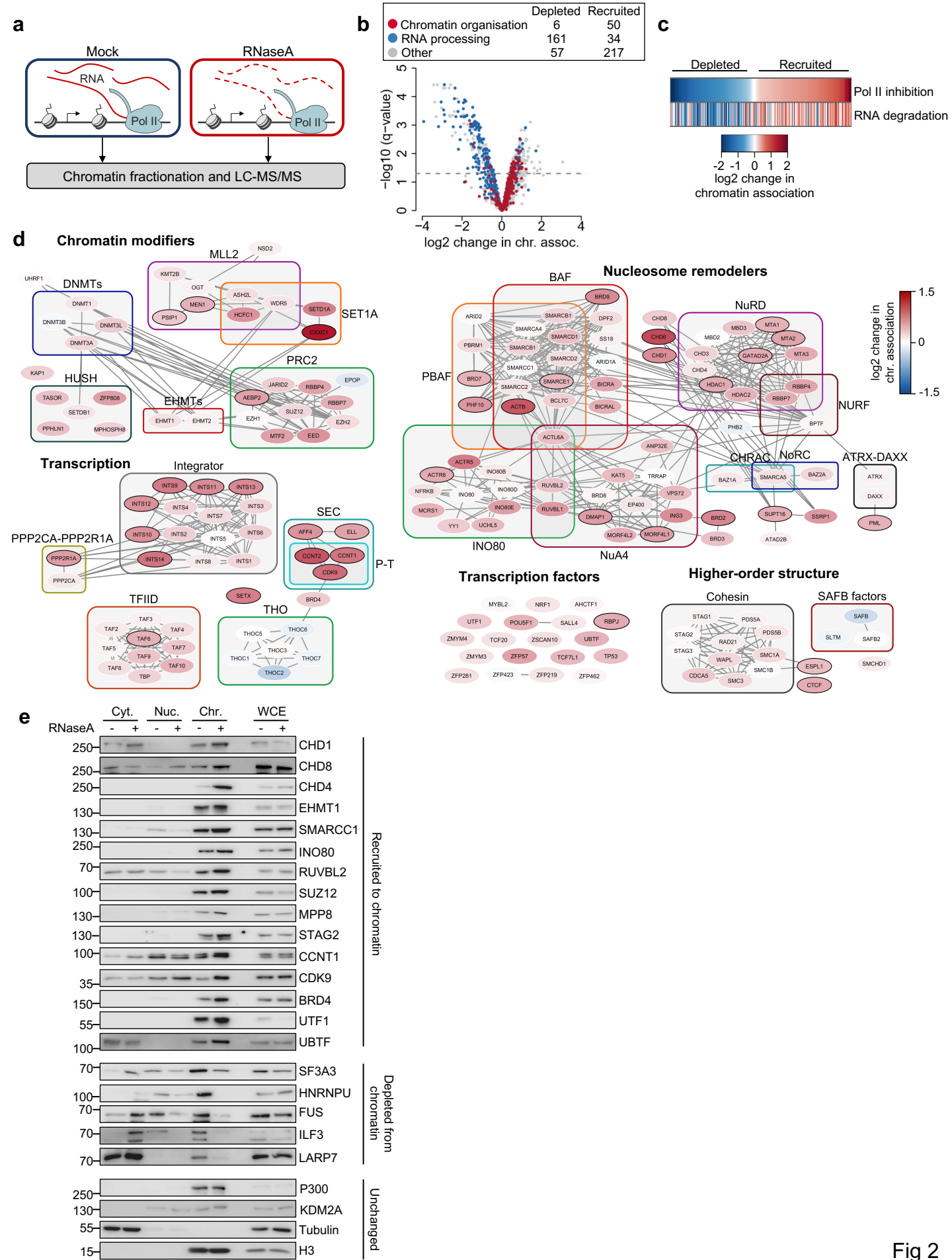y= −0.14x − 0.002
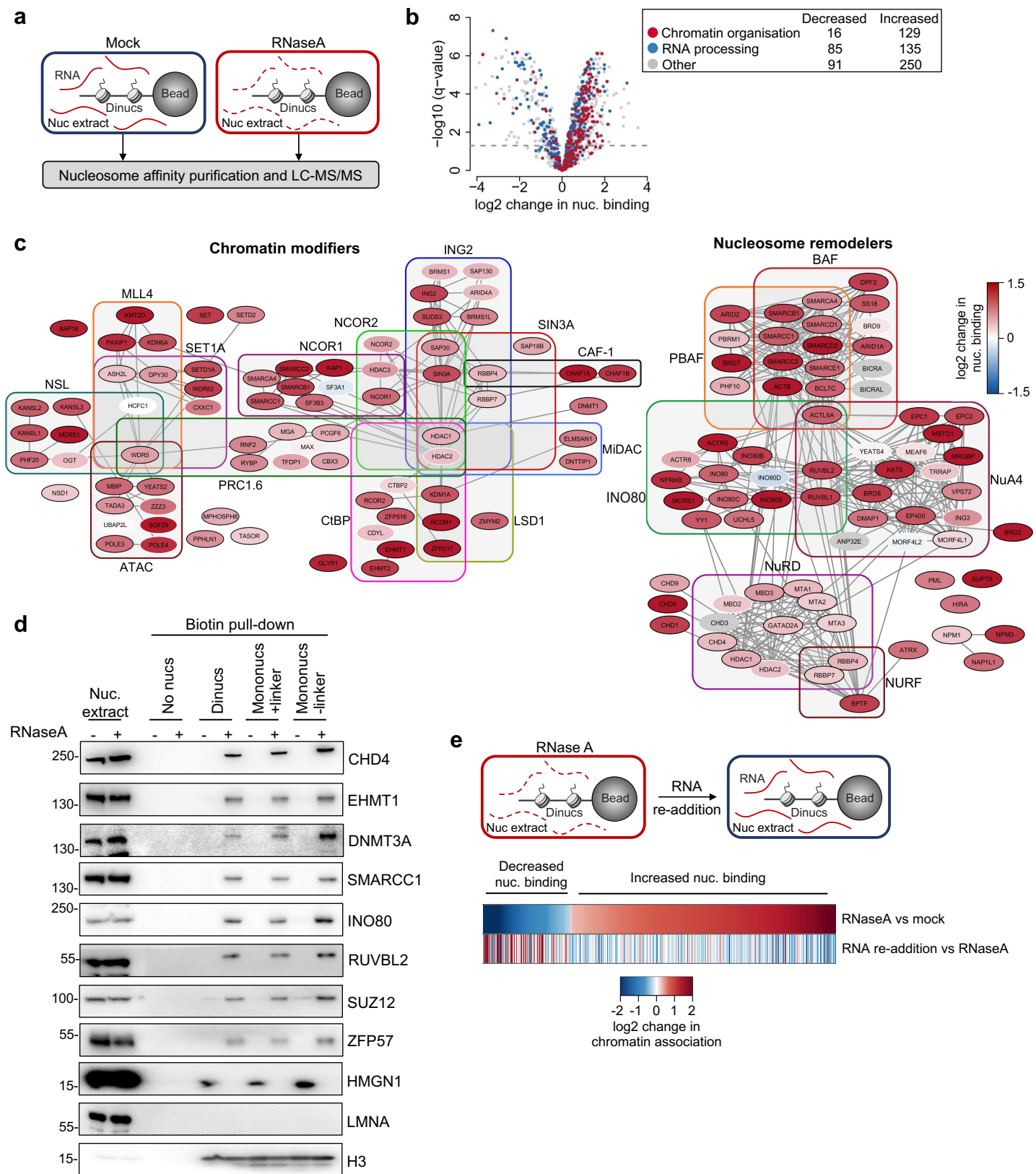r= −0.34, p=8.5e−16
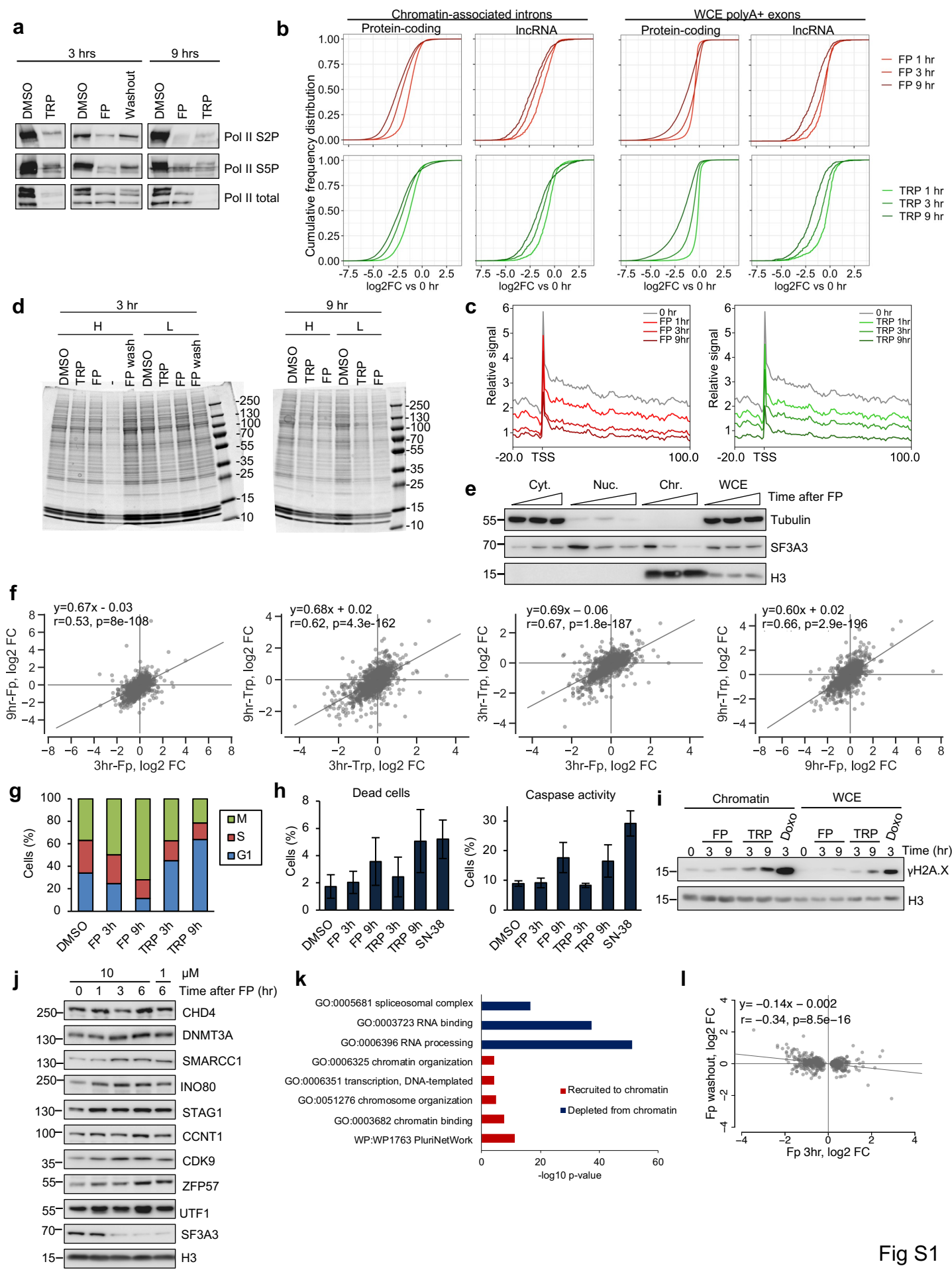
Fp washout, log2 FC / Fp 3hr, log2 FC

Fig S1

Figure S1. Effects of flavopiridol and triptolide treatment on the association of proteins with chromatin (related to Figure 1).

a. Immunoblots for serine-5 and serine-2 phosphorylated (S5P and S2P, respectively) and total Pol II in cells treated with DMSO, triptolide (TRP) or flavopiridol (FP) for 3 or 9 hrs. Washout indicates cells were treated with FP for 3 hrs, the media removed, cells washed, and incubated in media for a further 3 hrs. Protein concentration was measured by BCA and equal amounts loaded in each lane.

b. Cumulative frequency distribution of the change in abundance of chromatin-associated intronic transcripts or mature polyA+ exonic RNAs, divided into Ensembl protein-coding and lncRNA classifications, in cells treated with triptolide (green) or flavopiridiol (red) for 1, 3 or 9 hours compared to untreated cells. Median level of total chromatin-associated intronic RNA depletion from protein-coding genes: 1 hr FP 2.3-fold, 3 hrs FP 4.1-fold, 9 hrs FP 5.6 fold, 1 hr TRP 2.4-fold, 3 hrs TRP 3.8-fold, 9 hrs TRP 5.0 fold. Median level of total chromatin-associated intronic RNA depletion from lncRNA genes: 1 hr FP 2.3-fold, 3 hrs FP 3.6-fold, 9 hrs FP 4.7 fold, 1 hr TRP 1.6-fold, 3 hrs TRP 2.3-fold, 9 hrs TRP 3.1 fold. Median level of mature polyA+ exonic RNA depletion from protein-coding genes: 1 hr FP 1.4-fold, 3 hrs FP 1.4-fold, 9 hrs FP 2.3 fold, 1 hr TRP 1.1-fold, 3 hrs TRP 1.6-fold, 9 hrs TRP 3.0 fold. Median level of of mature polyA+ exonic RNA depletion from lncRNA genes: 1 hr FP 1.3-fold, 3 hrs FP 1.6-fold, 9 hrs FP 2.8 fold, 1 hr TRP 1.2-fold, 3 hrs TRP 1.8-fold, 9 hrs TRP 3.4 fold.

c. Metagene plots showing loss of nascent RNA (total chromatin-associated RNA) from chromatin at genes after treatment of cells with triptolide (left) or flavopiridol (right) for 1, 3 or 9 hours.

d. Silver stains of protein samples analysed by SILAC that were purified from cells treated for 3 or 9 hours with DMSO, flavopiridol (FP), triptolide (TRP) or after FP wash out (FP wash; details as for a). H: heavy labelled samples, L: light labelled samples, - : unused lane.

e. Immunoblots for control proteins (tubulin, SF3A3 and H3) in cytoplasmic (Cyt.), nucleoplasmic (Nuc.) and chromatin (Chr.) fractions and whole cell extract (WCE) from ESC cells treated with flavopiridol for 0, 3 and 9 hours.

f. Scatter plots showing the correlation between the effects of flavopiridol (Fp) and triptolide (Trp) at 3 and 9 hours, and between Fp and Trp treatments, on protein chromatin association. At a significance threshold of FDR<0.05, 444 proteins are recruited to chromatin after 9 hrs treatment with Fp and 399 proteins are recruited to chromatin after 9 hrs treatment with Trp; the overlap between these two sets is 281 proteins (p=5.86e-99). 375 proteins are depleted from chromatin after 9 hrs treatment with Fp and 331 proteins are depleted from chromatin after 9 hrs treatment with Trp; the overlap between these sets is 241 proteins (p=1.86e-167).

g. Proportion of cells at each stage of the cell cycle after 3 or 9 hrs treatment with flavopiridol (FP) or triptolide (TRP) (mean, n=3).

h. Proportion of dead cells (left, mean and S.D, n=3) and proportion of cells with caspase activity (right, mean and S.D, n=2) after treatment of cells with flavopiridol (FP), triptolide (TRP) or the TopoI inhibitor SN-38.

i. Levels of γH2A.X and total H3 in chromatin and WCE in ESC after 3 or 9 hrs treatment with flavopiridol (FP) or triptolide (TRP) or 3 hrs treatment with doxorubicin (Doxo), which induces DNA damage.

j. Immunoblots of representative proteins from Figure 1D showing their change in chromatin association after 1, 3 and 6 hrs treatment of ESC with 10 µM flavopiridol or 6 hrs treatment with 1 µM flavopiridol.

k. $-\log_{10}$ p-values (hypergeometric test) of selected Gene Ontology categories enriched in the set of proteins that are significantly recruited to chromatin (red) or depleted from chromatin (blue) in ESC after 9 hrs of treatment with flavopiridol and with triptolide. See Table S2 for full list.

l. Scatter plot of the data in Figure 1E showing a significant anti-correlation between the change in chromatin association after 3 hrs flavopiridol (Fp) treatment and the subsequent change in chromatin association 3 hrs after flavopiridol washout.
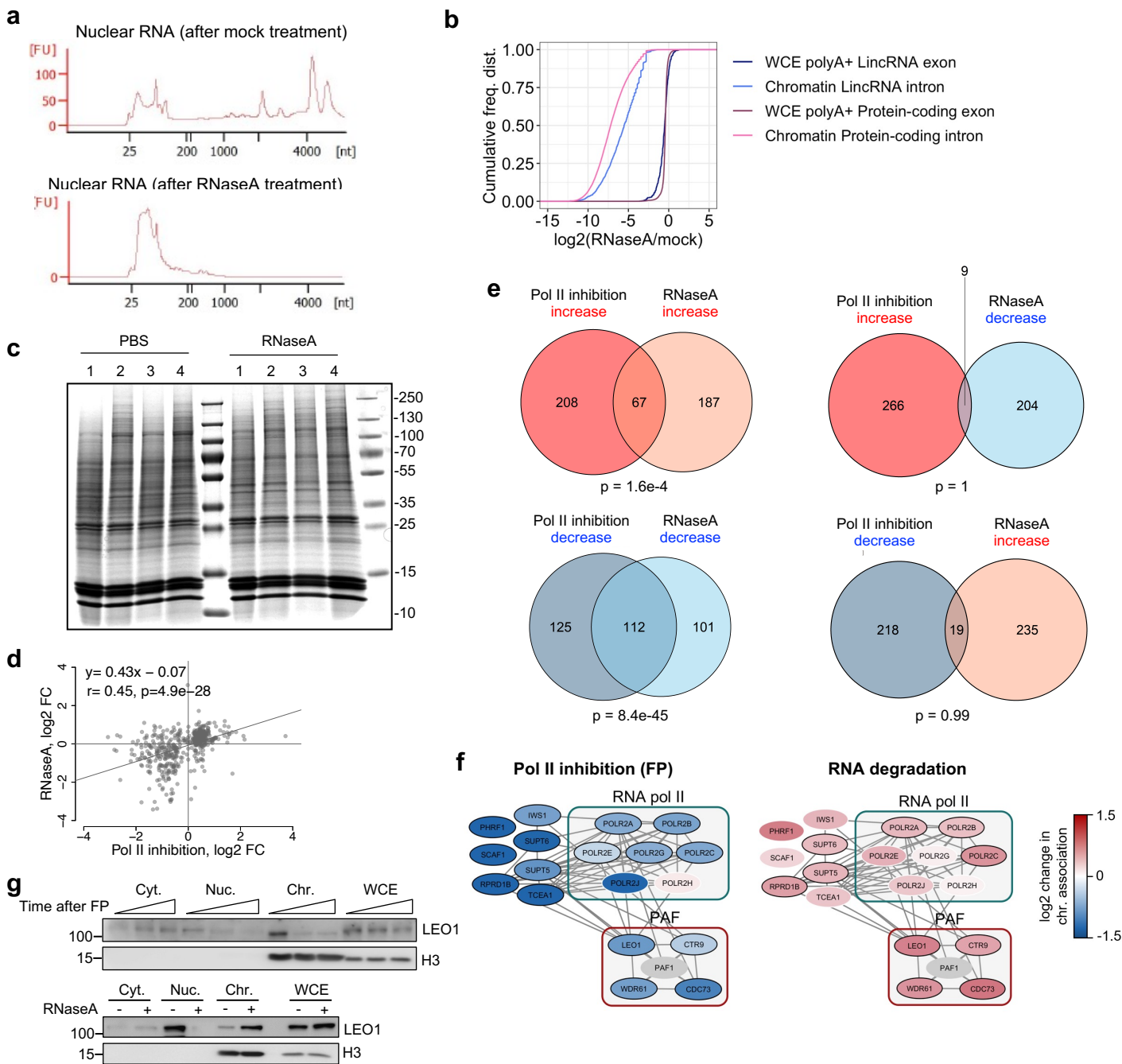
Figure S2. Effects of RNA degradation on the association of proteins in chromatin (related to Figure 2).

a. Bioanalyser traces of RNA in cells after mock treatment or treatment with RNaseA for samples analysed by LC-MS/MS.

b. Cumulative frequency distribution of the change in abundance of chromatin-associated intronic transcripts or mature polyA+ exonic RNAs, divided into Ensembl protein-coding and lncRNA classifications, in RNaseA versus mock-treated cells.

c. Silver stains of protein samples (replicates 1-4) analysed by LC-MS/MS that were purified from mock (PBS) or RNaseA-treated ESC.

d. Scatter plot of the data in Figure 2C showing a significant correlation between the change in chromatin association caused by Pol II inhibition (average of FP 9 hr and TRP 9 hr data) and the change in chromatin association caused by RNA degradation.

e. Venn diagrams depicting the overlap between the sets of proteins that show a significant (FDR<0.05) increase (red) or decrease (blue) in chromatin association after Pol II inhibition and the sets of proteins that show a significant increase or decrease in chromatin association after RNaseA treatment. The significance of each overlap is indicated (hypergeometric).

f. Proteins that show opposite changes in chromatin association after Pol II inhibition with flavopiridol versus RNA degradation. Proteins (ovals) are grouped by complex (identified by CORUM) and interactions between them (experimental evidence annotation in STRING) as lines. Change in the association of proteins with chromatin after treatment is indicated by color (scale on the right) with the color of the protein outline indicating significance (black FDR <0.05, white FDR>0.05).

g. Immunoblotting showing the opposite effect of flavopiridol (FP) treatment (0, 3 or 6 hrs; top) or treatment with (+) RNaseA (bottom) on the association of LEO1 with chromatin.
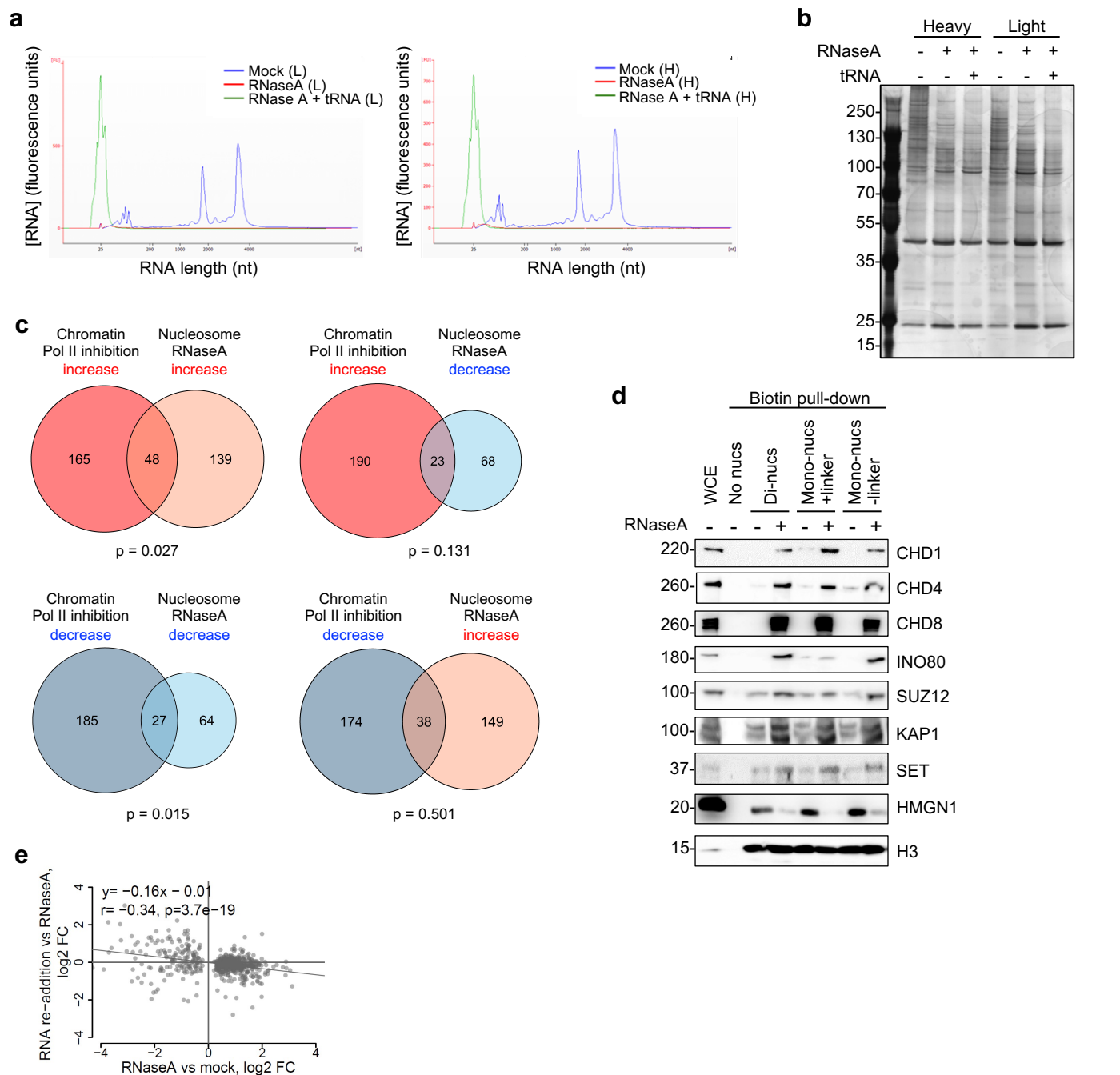
Fig S2

Figure S3. Effect of RNA degradation in nuclear extract on the interaction of proteins with nucleosomes (related to Figure 3).

a. Bioanalyser traces of RNA in heavy (H) or light (L) labeled nuclear extracts after mock treatment, treatment with RNaseA or treatment with RNaseA followed by tRNA addition. These samples were then used for SILAC-based analysis of nucleosome binding.

b. Silver stains of protein samples analysed by SILAC purified from nucleosomes incubated with heavy or light-labelled nuclear extracts after mock-treatment, RNaseA-treatment or treatment with RNaseA followed by tRNA addition.

c. Venn diagrams depicting the overlap between the sets of proteins that show a significant (FDR<0.05) increase (red) or decrease (blue) in chromatin association after Pol II inhibition and the sets of proteins that shown a significant (FDR<0.001) increase or decrease in nucleosome binding after RNase treatment of nuclear extract. The significance of each overlap is indicated (hypergeometric).

d. Immunoblots for proteins in biotinylated-nucleosome pull-downs (dinucleosomes, or mononucleosomes assembled with 187 bp or 147 bp DNA) from mock-treated (-) or RNaseA-treated (+) nuclear extracts.

e. Scatter plot of the data shown in Figure 3E showing a significant anti-correlation between the change in nucleosome binding upon RNA degradation and the change in nucleosome binding upon RNA re-addition.
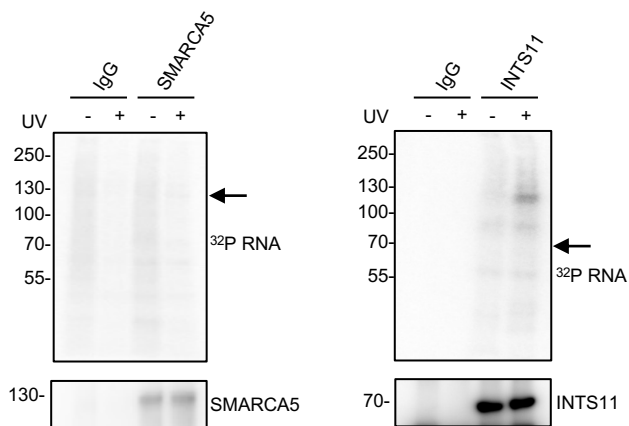
Fig S3

Figure S4. Proteins lacking detection of direct RNA binding in cells (related to Figure 4).
CLIP for SMARCA5, INST11 and non-specific IgG controls in ESCs showing the lack of enrichment of crosslinked RNA at the molecular weight of the two proteins. Autoradiograms of crosslinked ^{32}P-labelled RNA are shown at the top; the corresponding immunoblots, below. CLIP was performed with and without UV crosslinking. The arrow indicates the molecular weight of the protein of interest.
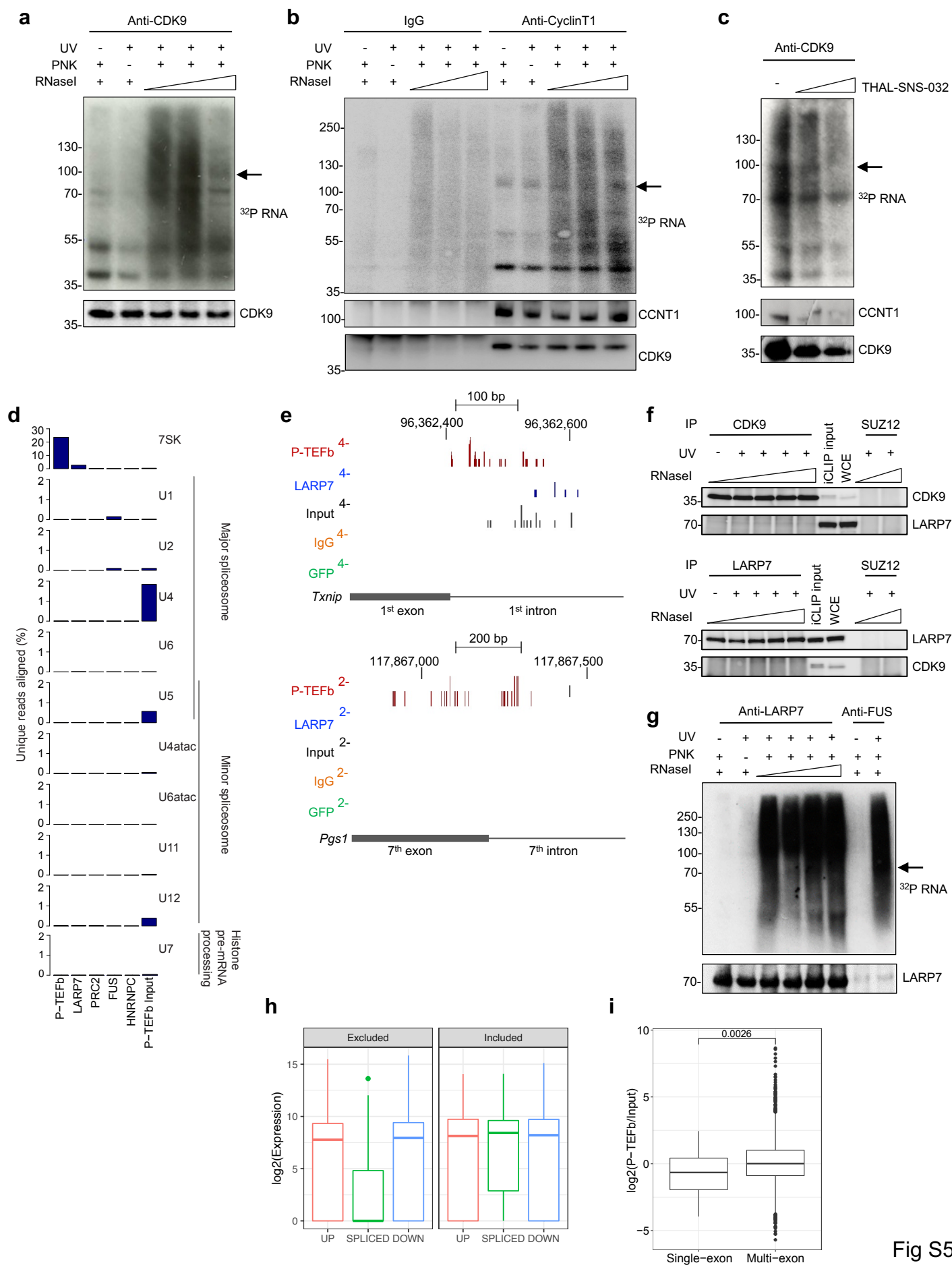
Fig S5

Figure S5. Direct interaction of P-TEFb with RNA in ESC (related to Figure 5).

a. SDS-PAGE for RNPs enriched by CLIP for CDK9 in ESCs. Autoradiograms of crosslinked ^{32}P-labelled RNA are shown at the top; the corresponding immunoblot, below. CLIP was performed with an antibody to CDK9 with and without UV crosslinking and polynucleotide kinase (PNK) and with increasing concentrations of RNase I (2, 4 and 10 U/ml). The molecular weight of CyclinT1 is indicated by the arrow.

b. SDS-PAGE for RNPs enriched by CLIP for CyclinT1 in ESCs. Autoradiograms of crosslinked ^{32}P-labelled RNA are shown at the top; the corresponding immunoblot, below. CLIP was performed with an antibody to CyclinT1 with and without UV crosslinking and polynucleotide kinase (PNK) and with increasing concentrations of RNase I (1, 5 and 20 U/ml). The molecular weight of CyclinT1 is indicated by the arrow.

c. SDS-PAGE for RNPs enriched by CLIP for CDK9 in ESCs with and without treatment with the CDK9 degrader THAL-SNS-038 (1 and 4 µM) for 1 hour. The molecular weight of CyclinT1 is indicated by the arrow.

d. Proportion of P-TEFb, LARP7 and P-TEFb input (data from this study) and PRC2, FUS and HNRNPC (data from Beltran et al., 2016) crosslinks (reads uniquely aligning with the genome) that are within 7SK and snRNAs.

e. Significant (FDR<0.05) P-TEFb, LARP7 and input crosslink sites (data from this study) and control IgG and GFP RNA crosslink sites (data from Beltran et al., 2019) at example 5'SS in ESC. Scales are denoted by the bars above.

f. Immunoblots for CDK9 and LARP7 in CDK9 and SUZ12 (top) and LARP7 and SUZ12 (bottom) CLIP immunoprecipitates, CLIP input material and whole cell extract**.**

g. SDS-PAGE for RNPs enriched by CLIP for LARP7 and FUS (positive-control) in ESCs. Autoradiograms of crosslinked ^{32}P-labelled RNA are shown at the top; the corresponding LARP7 immunoblot, below. CLIP was performed with and without UV crosslinking and polynucleotide kinase (PNK) and with increasing concentrations of RNase I (1, 2, 10 and 20 U/ml). The molecular weight of LARP7 is indicated by the arrow.

h. Boxplots showing the expression of the upstream (UP), alternatively spliced (SPLICED) and downstream (DOWN) exons for the sets of excluded and included exons at which P-TEFb and input crosslinking is plotted in Fig. 5B.

i. Boxplots showing the difference between the range of log2 ratios of P-TEFb versus input crosslinks between single-exon and multi-exon genes (p=0.0026, Student's t-test).
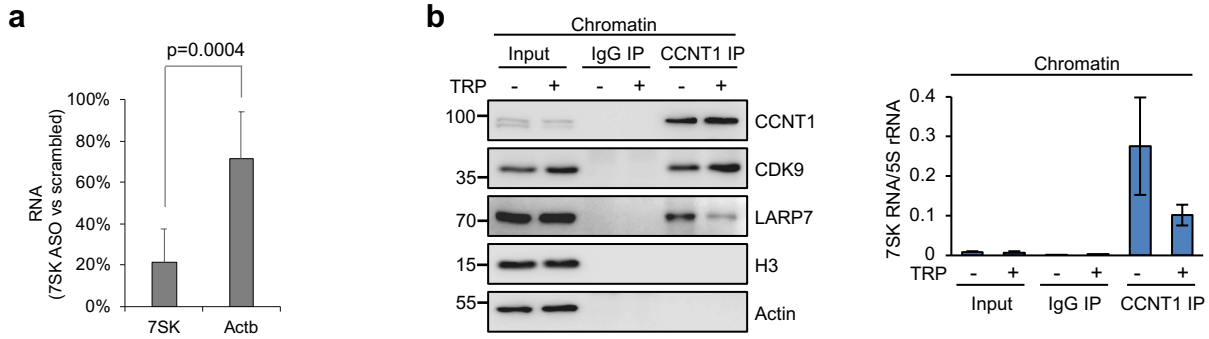
Figure S6. 7SK knockdown and interaction of P-TEFb with 7SK on chromatin (related to Figure 6).
a. Measurement (RT-qPCR) of the amount of 7SK and Actb RNA in ESC transfected with ASOs specific for 7SK RNA compared to ESC transfected with scrambled ASOs (mean and S.D., n=7, p=0.0004, Student's t-test).
b. Immunoblots (left) and RT-qPCR for 7SK relative to 5S RNA (right) in inputs and CCNT1 and IgG immunoprecipitates from the chromatin fraction of cells treated with (+) or without (-) triptolide for 6 hours. 3 independent experiments, representative immunoblot and mean and S.E. for RT-qPCR.